applied sciences

MDPI

Article

Expectorant Effects of *Atractylodes japonica* Koidz. ex Kitam Root Extracts on Particulate Matter-Induced Pulmonary Injury in Mice

Junho Lee [1,†], Sana Mansoor [2,†], Jeongjun Lee [3], Hunsuk Chung [3], Young-Sam Kwon [1], Khawaja Muhammad Imran Bashir [2,4], Jae-Suk Choi [2,*] and Sae-Kwang Ku [5,*]

1 Department of Veterinary Surgery, College of Veterinary Medicine, Kyungpook National University, Daegu 41566, Republic of Korea; 2009045032@knu.ac.kr (J.L.); kwon@knu.ac.kr (Y.-S.K.)
2 Department of Seafood Science and Technology, The Institute of Marine Industry, Gyeongsang National University, Tongyeong 53064, Republic of Korea; sanamansoorahmad@gmail.com (S.M.); imranbashir@gnu.ac.kr (K.M.I.B.)
3 GAPI BIO Co., Ltd., Hwaseong 18622, Republic of Korea; orglab@gapibio.co.kr (J.L.); hunsukchung@dongbangchem.co.kr (H.C.)
4 German Engineering Research and Development Center for Life Science Technologies in Medicine and Environment, Busan 46742, Republic of Korea
5 Department of Anatomy and Histology, College of Korean Medicine, Daegu Haany University, Gyeongsan 38610, Republic of Korea
* Correspondence: jsc1008@gnu.ac.kr (J.-S.C.); gucci200@dhu.ac.kr (S.-K.K.); Tel.: +82-55-772-9142 (J.-S.C.); +82-53-819-1549 (S.-K.K.)
† These authors contributed equally to this work.

Abstract: This study investigated the growing environmental concern of particulate matter (PM)-induced pulmonary injury and explored novel preventive strategies. In particular, it evaluated the protective effects of *Atractylodes japonica* Koidz. ex. Kitam root extract (AJ), which is known for its anti-inflammatory and antioxidant properties, against $PM_{2.5}$-induced subacute pulmonary injuries in Balb/c mice. The experimental design involved administering AJ at a concentration from 400 to 100 mg/kg over a ten-day period, with comparisons made to the mucolytic agent ambroxol hydrochloride (AX). The results revealed that AJ significantly alleviated $PM_{2.5}$-induced pulmonary injuries, mucus overproduction, and respiratory acidosis in a dose-dependent manner. Notably, body surface redness was reduced by up to 55% at a concentration of 100 mg/kg compared to the control. These effects were evidenced by reduced mRNA expression of the mucus-associated genes MUC5B and MUC5AC and increased concentrations of substance P (up to 475%) and acetylcholine (up to 355%) in the lungs at 400 mg/kg, compared to the intact vehicle control. Particularly, the 400 mg/kg dose of AJ demonstrated comparable effectiveness to AX, highlighting its potent mucolytic and expectorant activities. The results of this study highlight the fact that AJ could act as a promising alternative for respiratory protection, with potential applications as a functional food ingredient. This study substantiates AJ's role in enhancing respiratory health, emphasizing its capacity as a candidate for further development into therapeutic agents against toxic environmental exposure.

Keywords: antioxidant activity; anti-inflammatory; *Atractylodes japonica*; herbal medicine; mucolytic expectorant; respiratory protection

check for updates

Academic Editor: Ewelina Zielińska

Received: 14 November 2024
Revised: 16 December 2024
Accepted: 25 December 2024
Published: 26 December 2024

Citation: Lee, J.; Mansoor, S.; Lee, J.; Chung, H.; Kwon, Y.-S.; Bashir, K.M.I.; Choi, J.-S.; Ku, S.-K. Expectorant Effects of *Atractylodes japonica* Koidz. ex Kitam Root Extracts on Particulate Matter-Induced Pulmonary Injury in Mice. *Appl. Sci.* **2025**, *15*, 99. https://doi.org/10.3390/app15010099

Copyright: © 2024 by the authors. Licensee MDPI, Basel, Switzerland. This article is an open access article distributed under the terms and conditions of the Creative Commons Attribution (CC BY) license (https://creativecommons.org/licenses/by/4.0/).

1. Introduction

Air pollution has emerged as a critical public health and environmental challenge, particularly in East Asian countries such as Korea, Japan, and China. The rapid industrial-

ization and urbanization in these regions have led to the increased prevalence of fine dust and particulate matter (PM), notably $PM_{2.5}$. These fine particles, with a diameter of 2.5 µm or less, have been implicated in numerous adverse health effects, and they significantly contribute to both regional and global climate change. In urban centers like Beijing, the capital city of China, the air is often thick with smog primarily composed of $PM_{2.5}$, arising from a combination of natural and human-made sources [1–3]. Natural sources include dust storms originating from the Loess Plateau and Mongolian deserts, while anthropogenic sources encompass industrial emissions, vehicular exhaust, and coal combustion [4]. Beijing, the capital city of China, exemplifies this issue, as it is often shrouded in dense smog primarily comprised of $PM_{2.5}$. Despite efforts initiated post-2008 Olympics to mitigate pollution, Beijing remains one of the most polluted cities globally [5].

The composition of $PM_{2.5}$ is intricate, comprising a diverse array of substances. It includes mineral dust and endotoxins alongside organic pollutants such as alkanes, fatty acids, hopanes, polycyclic aromatic hydrocarbons (PAHs), and dicarboxylic acids. Inorganic constituents like sulfates and nitrates are also significant components [6]. Recent studies have highlighted that organic aerosols and nitrates constitute major fractions of $PM_{2.5}$ in various Chinese cities [7,8]. Among the components, organic matter is the most prevalent at 35.3%, followed by nitrate at 22.0%, sulfate at 9.2%, and ammonium at 7.8% [8]. The fine nature of $PM_{2.5}$ allows these particles to penetrate deep into the respiratory system, reaching the alveoli and possibly entering the bloodstream. This penetration can bypass the body's natural defense mechanisms, resulting in significant tissue damage and various cardiopulmonary complications [1–3,9].

The health impacts of $PM_{2.5}$ are profound and multifaceted. Prolonged exposure to these particles is associated with exacerbated symptoms of respiratory diseases such as asthma, a long-term inflammatory disorder of the airways. Asthma affects millions globally and poses a significant public health challenge [10]. The accumulation of $PM_{2.5}$ in the lower respiratory tract is associated with heightened inflammation and oxidative stress, marked by increased levels of reactive oxygen species (ROS) and pro-inflammatory cytokines [5,11]. This oxidative stress can overwhelm the antioxidant defenses of respiratory epithelium, resulting in cellular injury and inflammation [5]. Additionally, $PM_{2.5}$ exposure can disrupt endothelial barriers and cause vascular leakage via the p38 MAPK pathway, alongside increasing mucin production [2,3].

Cough, a prevalent symptom of respiratory tract disorders, can be particularly distressing. It is classified into productive (chesty) or non-productive (dry) categories [12]. Effective management of a productive cough often necessitates treatments that facilitate mucus mobilization and clearance from the respiratory tract [13]. Expectorants play a crucial role in this process by enhancing the secretion and hydration of respiratory mucus, thus easing its clearance [14,15]. The expectorant effect of drugs has been evaluated using various experimental approaches, such as phenol red secretion technique on mouse trachea, which provides a simple yet effective method for assessing mucus secretion [16–19]. While antitussive medications are effective in treating dry coughs, they may be less efficacious for wet coughs unless they possess expectorant properties [13]. Inflammation is a crucial factor in the pathogenesis of numerous respiratory disorders. Consequently, drugs that combine antitussive, expectorant, and anti-inflammatory properties are believed to offer substantial protective effects against a variety of respiratory conditions, particularly those arising from toxic environmental exposures [16–19].

The search for new preventive and therapeutic strategies is crucial to protecting human respiratory systems from PM-induced pulmonary damage. In this context, natural products, known for their physiologically active compounds, demonstrate outstanding anti-inflammatory and antioxidant properties with comparatively fewer adverse effects

than synthetic drugs [20,21]. This has sparked considerable interest in the development of respiration-protective medications derived from natural sources, especially for addressing lung injuries induced by $PM_{2.5}$ exposure. Medicinal herbs, in particular, are garnering significant attention owing to their possible health advantages and bioactive compounds [21,22]. Our previous reports have shown the anti-tussive, anti-inflammatory, and expectorant effects of several plant extracts, including *Adenophora triphylla*, Asian pears, and Kyeongok-go, which have been tested across various mouse models [17–19,23]. Kyeongok-go, a traditional herbal preparation, combines ingredients such as *Poria cocos*, *Rehmannia glutinosa*, and honey [17]. The progress in creating respiratory-protective medications from natural substances is moving forward in various asthma-induced animal models, such as OVA-induced C57BL/6 mice [24]. Although ambroxol, a well-established mucolytic agent, has been used clinically for over four decades to manage respiratory disorders by acting as both a mucoactive agent and possessing anti-inflammatory and antioxidant properties [25]. Its use is restricted in certain populations, particularly those with gastric ulcers or during the first trimester of pregnancy [26]. This highlights the need for alternative therapies that are both effective and safe.

Among the diverse array of natural products, *Atractylodes japonica* Koidz. ex Kitam, commonly known as Sapju in Korea, stands out as a prominent traditional medicinal herb extensively consumed in East Asian countries [27–30]. This herb has reported a variety of bioactive characteristics, including anti-obesity, anti-inflammatory, and antioxidant effects [27–30]. Although previous reports have exhibited that *Atractylodes* may exert its favorable effects through mechanisms involving potent expectorant, antioxidant, and anti-inflammatory activities [23,31–33], there are no comprehensive reports on the effects of Atractylodis Rhizoma (root of *A. japonica*) extracts against $PM_{2.5}$-induced pulmonary injuries. This research seeks to explore the dose-dependent expectorant effect of Atractylodis Rhizoma extracts on $PM_{2.5}$-induced pulmonary injuries in a mouse model that simulates human fine dust-induced pulmonary disorders [1–3]. By utilizing the phenol red secretion method, this research evaluates the efficacy of *A. japonica* in comparison with ambroxol [16,17]. Through this investigation, we seek to validate its potential as a novel respiratory therapeutic substance or functional food component, offering a promising alternative to combat the adverse effects of air pollution on respiratory health.

2. Materials and Methods

2.1. Animal Care and Management

Eighty-eight healthy 6-week-old male SPF/VAF inbred Balb/cAnNCrlOri (Balb/c) mice were obtained from OrientBio, Seongnam, Republic of Korea. The selection of experimental animal model was based on our previous studies [2,3]. A total of 1.5 times the required number of Balb/c mice (88 in total) were initially prepared to allow for selection. Ten mice per group were chosen based on respiratory abnormalities and body weight variations after a 10-day acclimatization period. They were housed in groups of four within polycarbonate cages under controlled environment conditions throughout the experimental period. The temperature was maintained between 20–25 °C, and humidity levels were kept at 30–35%. The light and dark cycle was regulated to 12 h each. Water and feed (38057; Purinafeed, Seongnam, Republic of Korea) were provided ad libitum. For the experimental setup, ten mice per group resulted in a total of six groups. This included 50 $PM_{2.5}$-induced pulmonary injured mice and 10 intact mice, selected based on their body weights measured one day prior to the first $PM_{2.5}$ intranasal instillation after 10 days of acclimatization. The average weight for intact mice was 20.73 ± 1.46 g (range: 17.70–22.90 g), and, for $PM_{2.5}$-induced pulmonary injured mice, it was 20.72 ± 1.30 g (range: 18.40–23.80 g). These mice were divided into six experimental groups, as outlined below.

1. Intact (vehicle) control: Distilled water (10 mL/kg) was orally administered to mice, with 0.1 mL/kg saline given intranasally.
2. $PM_{2.5}$ (vehicle) control: Distilled water (10 mL/kg) was orally administered to mice, with 1 mg/kg of $PM_{2.5}$ given intranasally.
3. AX_{250}: Ambroxol hydrochloride (AX; 250 mg/kg) was orally administered to mice, with 1 mg/kg of $PM_{2.5}$ (1 mg/kg) given intranasally.
4. AJ_{400}: *Atractylodes japonica* extract (AJ; 400 mg/kg) was orally administered to mice, with 1 mg/kg of $PM_{2.5}$ given intranasally.
5. AJ_{200}: AJ (200 mg/kg) was orally administered to mice, with 1 mg/kg of $PM_{2.5}$ given intranasally.
6. AJ_{100}: AJ (100 mg/kg) was orally administered to mice, with 1 mg/kg of $PM_{2.5}$ given intranasally.

This animal study complied with international standards regarding laboratory animal use and welfare and was approved by the Institutional Animal Care and Use Committee at Daegu Haany University, Gyeongsan, Republic of Korea [Approval No.: DHU2022-016, approved on 22 February 2022].

2.2. Induction of Pulmonary Injuries by $PM_{2.5}$ in Mice

Subacute pulmonary injuries in the mice were induced through intranasal administration of $PM_{2.5}$ suspensions (NIST 1650B; Sigma-Aldrich, St. Louis, MO, USA), prepared at a dose of 10 mg/mL in physiological saline. The instillation was performed twice, with a 48 h interval, on Day 0 and Day 2, one hour before the oral administration of the experimental substances. The volume administered was 0.1 mL/kg, equivalent to a concentration of 1 mg/kg [1–3]. To prevent agglomeration of the $PM_{2.5}$ particles, the suspensions were sonicated for 30 min (5210; Branson, St. Louis, MO, USA) before each installation on Day 0 and Day 2.

2.3. Test Substance Preparations and Administration

The test substance, a reddish-brown powder of Atractylodis Rhizoma (root of *Atractylodes japonica* Koidz. ex Kitam) extracts (AJ), was standardized and provided by NUTRACORE, Suwon, Republic of Korea. It exhibited solubility in distilled water at room temperature, reaching a concentration of up to 40 mg/mL. AJ specimens were archived in the herbarium of the Medical Research Center for Herbal Convergence on Liver Disease at Daegu Haany University, Gyeongsan, Republic of Korea. Additionally, Ambroxol hydrochloride (AX; 23828-92-4; Sigma-Aldrich, St. Louis, MO, USA) was employed as a potent standard drug, consistent with previous studies [17–19].

A dosage of AJ at 400, 200, and 100 mg/kg was given orally once a day for 10 days through gastric gavage. Similarly, the reference drug AX was administered at 250 mg/kg once daily for 10 days. To maintain consistent restraint stress from oral gavage, equal volumes of distilled water, the vehicle, were administered orally to both the intact vehicle and $PM_{2.5}$ control mice.

The dosage level of AX (250 mg/kg) was chosen based on recommendations from other studies on in vivo efficacy [17–19]. The middle dosage of AJ, 200 mg/kg, was decided based on results from our prior efficacy tests on $PM_{2.5}$-induced pulmonary injured mice [17–19,23,32]. The highest (400 mg/kg) and lowest (100 mg/kg) dosages of AJ were chosen using a common ratio of 2, consistent with our previous dose-dependent pulmonary protective activity tests on $PM_{2.5}$-induced subacute lung damage in mice [23].

2.4. Test Substance Analysis by High-Performance Liquid Chromatography

The content of atractylenolide III in the root extracts of *A. japonica* (AJ extracts) was measured using an Agilent 1260 Infinity II high-performance liquid chromatography (HPLC) system (Agilent Technologies, Inc., Santa Clara, CA, USA). This system featured a UV–visible detector and employed a Unison US-C_{18} column (dimensions: 4.6 mm × 250 mm, particle size: 5 μm; Peakman^{SP} Co., Ltd., Hanam, Republic of Korea). Both the AJ extract and the standard atractylenolide III were dissolved in methanol and subsequently filtered using a 0.45 μm filter disc. The column temperature was kept at a constant 25 °C throughout the analysis, with the detection of atractylenolide III occurring at 224 nm wavelength. The mobile phase consisted of acetonitrile and 0.05% trifluoroacetic acid. Detailed HPLC analytical conditions are listed in Table S1. For calibration, standard atractylenolide III (BF-A2011) obtained from Biofron Inc., Fullerton, CA, USA, was employed as a reference. The sample was injected at a volume of 10 μL, and the flow rate was set at 1.0 mL/min. Quantification was performed by comparing the relative peak area to that of the standard, allowing for determination based on peak area and concentration relationships.

2.5. Changes in Body Weights

Body weight changes were recorded once daily, beginning one day prior to the initial $PM_{2.5}$ nasal instillation and test article oral administration, continuing throughout the entire experimental period. Measurements were conducted using an electronic balance (XB320M; Precisa Instrument, Dietikon, Switzerland). To minimize individual variations, body weight gains were calculated from the first day of oral administration of the test article to 24 h after the last (10th) administration, using Equation (1).

$$\text{Body Weight Gains (g) over the 10-Day Experimental Period} = \text{Body weight 24 h after the final oral administration of the test article} - \text{Body weight on the day of } PM_{2.5} \text{ nasal instillation and test article oral administration} \quad (1)$$

2.6. Phenol Red (pH-Sensitive Dye) Secretion Test

Tracheal secretions were assessed via a single intraperitoneal injection of a 5% phenol red solution (143-74-8; Junsei Chemical Co., Ltd., Tokyo, Japan), which was solubilized in saline (*w*/*v*) at a dosage of 10 mL/kg, provided 24 h after the final supply of test substance. Thirty minutes after the injection of the phenol red solution, all mice were euthanized by cervical dislocation, ensuring the trachea remained intact. Body surface redness was recorded with a digital camera (FinePix S700; Fujifilm, Tokyo, Japan) under anesthesia induced with from 2 to 3% isoflurane (Hana Pharm. Co., Hwasung, Republic of Korea), utilizing a rodent inhalation anesthesia apparatus (Surgivet, Waukesha, WI, USA) and a rodent ventilator (Model 687; Harvard Apparatus, Cambridge, UK). Subsequently, the trachea was carefully dissected from the thyroid cartilage to the main stem bronchi. Trachea lavage fluid (TLF) was prepared by sonicating for 15 min (Branson Ultrasonics) and adding 1 mL of 5% $NaHCO_3$ solution to normal saline. Optical density was assessed at 546 nm with a microplate reader (Model Sunrise; Tecan, Männedorf, Switzerland) [16–19].

2.7. Body Surface Inspections

At 24.5 h after the last (10th) test article oral administration and 30 min after phenol red solution injection, body surface inspections were conducted and documented using a commercial digital camera (Fujifilm) under inhalation anesthesia. The intensity of redness in the captured images was quantified with a computer-based image analyzer (iSolution FL; version 9.1; IMT i-solution Inc., Burnaby, BC, Canada) and expressed as a percentage relative to the intact control.

2.8. Measurements of Lung Weights

After dissecting the trachea, the lungs from each mouse were isolated while the animals were under inhalation anesthesia. Their absolute wet weights were measured with an electronic balance (Precisa Instrument). To account for individual body weight variations, relative lung weights (expressed as a percentage of body weight) were calculated using the body weight at the time of sacrifice and the absolute lung weight, as described in Equation (2).

$$\text{Relative Lung Weights (\% of body weight)} = [\text{Absolute lung wet weight}/\text{Body weight at sacrifice (24 h after the last test substance oral administration)} \times 100] \quad (2)$$

2.9. Lung Gross Inspections and ELISA Assay

After weighing the isolated lungs, a 3-0 sterilized nylon ligature (NB 324; AILEE, Busan, Republic of Korea) was applied to the left secondary bronchus. The right lung lobes (lower, middle, and upper) were designated for analyses of acetylcholine (ACh) and substance P content, as well as for real-time RT-PCR analysis. The left lobe was reserved for histopathological and gross examinations. Gross observations were documented using a digital camera (Fujifilm), and the percentage of congested regions in the images of the left lobe was assessed with an image analyzer (iSolution Inc.).

For preparing lung tissue homogenates, the right upper, middle, and lower lung lobes were homogenized with a bead beater (TacoTMPre; GeneResearch Biotechnology Corp., Taichung, Taiwan) and an ultrasonic cell disruptor (KS-750; Madell Technology Corp., Ontario, CA, USA) in equal volumes to normal saline. The homogenates were kept at −150 °C in an ultra-deep freezer (MDF-1156; Sanyo, Tokyo, Japan) until further use. The tissue homogenates were subjected to centrifugation at 12,500 rpm for 30 min at 4 °C using a cryocentrifuge (Labocene 1236 MGR; Gyrozen, Daejeon, Republic of Korea). The levels of ACh and substance P in the supernatant were assessed using mouse ACh (MBS284198; Mybiosource, San Diego, CA, USA) and substance P (MBS843429; Mybiosource, San Diego) ELISA kits, following the manufacturer's instructions. Optical density readings were taken at 450 nm with a microplate reader.

2.10. Real-Time RT-PCR

The mRNA expressions of mucus-producing genes such as MUC5B and MUC5AC were quantified with a real-time RT-PCR machine, as outlined in earlier studies [34,35]. RNA was isolated with a Trizol RNA isolation kit (Invitrogen, Carlsbad, CA, USA), and the quality and concentration of isolated RNA were measured with the Real-Time PCR System (CFX96TM; Bio-Rad, Hercules, CA, USA). The RNA samples were processed with a recombinant DNase I DNA Removal Kit (Cat No. AM1906; Thermo Fisher Scientific Inc., Rockford, IL, USA) to remove any contaminating DNA. The RNA was reverse-transcribed using the High-Capacity cDNA Reverse Transcription Kit (4368813; Thermo Fisher Scientific Inc., Rockford, IL, USA). PCR analyses were conducted using the ABI Step One Plus Sequence Detection System (Applied Biosystems, Foster City, CA, USA). The PCR cycling conditions included an initial pre-denaturation step at 95 °C for 1 min, followed by 50 cycles of denaturation for 15 s, annealing at 55–65 °C for 20 s, and extension at 72 °C for 30 s. β-actin RNA was used as a standard to check tissue integrity in the tested samples. PCR primer sequences are provided in Table S2. For quantification, the intact control lung tissue served as the baseline, and the relative expressions of MUC5AC and MUC5B were determined utilizing the $2^{-\Delta\Delta Cq}$ method [36].

2.11. Histopathology

Equal sections from the left lobe of each lung were trimmed crosswise, with one part taken from each lung sample. All trimmed sections of the left lung lobe were then re-fixed in 10% neutral buffered formalin for a minimum of 24 h. Paraffin blocks were prepared by a tissue processor (Shandon Citadel 2000; Thermo Scientific, Waltham, MA, USA) and an embedding center (Shandon Histostar; Thermo Scientific, Waltham, MA, USA). Sections were sliced to a thickness of 3–4 µm with a microtome (RM2255; Leica Biosystems, Nussloch, Germany), yielding four serial sections per paraffin block. Representative sections were hematoxylin and eosin (H&E) stained for general histopathology and with Periodic Acid-Schiff (PAS) for identifying mucus-producing goblet cells, following established protocols [17–19,37]. Two additional serial sections were used for avidin-biotin-peroxidase complex (ABC)-based immunohistochemical staining targeting cleaved caspase-3 and cyclooxygenase-2 (COX-2). Histological profiles were examined using a light microscope (Model Eclipse 80i; Nikon, Tokyo, Japan) coupled with a camera system (ProgRes™ C5; Entoptic Optical Systems GmbH, Jena, Germany) and an image analyzer. The analysis was conducted without knowledge of group distribution.

For detailed observations, mean alveolar surface area (ASA, %/mm^2) reflecting pulmonary function and gas exchange capacities [17–19,24,37], mean alveolar septal thickness (µm), and numbers of PAS+ mucus-producing inflammatory cells in alveolar regions (cells/mm^2), on the secondary bronchus, were calculated by an image analysis program [17–19,24,37,38]. Histological fields were chosen from the upper areas of the secondary bronchus, with at least one field per left lung tissue, resulting in a minimum of 10 histological lung areas per group.

2.12. Immunohistochemistry

Changes in cleaved COX-2 and caspase-3 immunoreactive cells were examined using ABC-based immunohistochemical techniques with primary antibodies (as detailed in Table S3) and suitable peroxidase substrate and ABC kits (Vector Labs, Burlingame, CA, USA). The activity of endogenous peroxidase was inhibited by incubating the sections in methanol with 0.3% H_2O_2 for 30 min. Non-specific binding was prevented by treating with a horse serum blocking solution for 1 h in a humidity chamber, following heat-induced epitope retrieval in 10 mM citrate buffer (pH 6.0) [39,40]. The primary antisera were applied overnight at 4 °C in a humidity chamber. This process was followed by incubation with ABC reagents and a biotinylated universal secondary antibody for 1 h at room temperature in a humidity chamber. The sections were then treated with a peroxidase substrate kit for 3 min at room temperature. Between each step, all sections were rinsed thrice with 0.01 M phosphate-buffered saline (PBS). Cells exhibiting over 20% immunoreactivity were classified as positive. The density of cleaved COX-2 and caspase-3 immunolabeled cells in in the mucosa of the secondary bronchus, around the alveolar septum, and the lung parenchyma, was quantified in cells/mm^2 using a computer-assisted automated image analyzer [39,40]. The histopathologist conducting the analysis was blinded to group distribution.

2.13. Statistical Analyses

All numerical data are presented as means ± standard deviation (S.D.) for ten mice. Multiple comparisons among different dose groups were performed. The homogeneity of variances was evaluated using the Levene test. If the Levene test did not show significant deviations from variance homogeneity, a one-way analysis of variance (ANOVA) was used, followed by Tukey's Honest Significant Difference (THSD) test to identify significant pairwise differences. Conversely, if the Levene test indicated significant deviations from

variance homogeneity, Dunnett's T3 (DT3) test was employed to determine significant differences [41]. Statistical analyses were performed using SPSS version 18.0 (SPSS Inc., Chicago, IL, USA), and a p-value of less than 0.05 was regarded as statistically significant. Additionally, percent changes between the $PM_{2.5}$ control and intact vehicle group were measured to evaluate the severity of pulmonary injuries caused by intranasal instillation of $PM_{2.5}$. Percent variations between the $PM_{2.5}$ control and the AJ- and AX-administered mice were also computed to assess efficacy, according to Equations (3) and (4), based on earlier established methods [37,42,43].

$$\text{Percentage Changes Compared with Intact Vehicle Control (\%)} = [(\text{Data of } PM_{2.5} \text{ control} - \text{Data of intact vehicle control mice}/\text{Data of intact vehicle control mice}) \times 100] \quad (3)$$

$$\text{Percentage Changes Compared with } PM_{2.5} \text{ Control (\%)} = [(\text{Data of test material or reference-treated mice} - \text{Data of } PM_{2.5} \text{ control mice}/\text{Data of } PM_{2.5} \text{ control mice}) \times 100] \quad (4)$$

3. Results

3.1. Atractylenolide III Concentration in AJ Extract

Through HPLC analysis, the concentration of atractylenolide III in the AJ extract was determined to be 0.56 mg per gram. This quantification was achieved by assessing the relative peak area in comparison to the concentration and standard peak area, as illustrated in Figure S1.

3.2. Variations in Body Weight and Weight Gains

Throughout the 10-day experimental period, no substantial changes were noted in body weight and weight gains in $PM_{2.5}$-intranasally instilled mice compared to the intact vehicle control mice. Similarly, mice administered with three different dosages of the test substance, AJ (400, 200, and 100 mg/kg), and the standard drug, AX (250 mg/kg), did not reveal significant variations in body weights and gains compared to the $PM_{2.5}$ control mice (Figure S1). The body weight gains over the 10 days in the $PM_{2.5}$ control mice changed by 3.28% compared to the intact vehicle control. Variations in body weight gains for AX (250 mg/kg), AJ (400, 200, and 100 mg/kg) administered mice were 4.23%, −4.76%, −1.59%, and 0.53%, respectively, compared to the $PM_{2.5}$ control.

3.3. Effects on Trachea pH-Sensitive Phenol Red Secretions

Significant increases in tracheal lavage fluid (TLF), optical density (OD) values, and phenol red secretions were noted in the $PM_{2.5}$ control mice compared to the intact vehicle. Significant and dose-dependent elevations in trachea phenol red secretions were also noted in all three doses of AJ (400, 200, and 100 mg/kg) groups compared to the $PM_{2.5}$ control. Notably, AJ (400 mg/kg) revealed promising increases in TLF OD values and phenol red secretions in $PM_{2.5}$-induced subacute lung-damaged Balb/c mice, comparable to AX (250 mg/kg; Figure 1). The TLF OD values for phenol red secretions in the $PM_{2.5}$ control differed by 31.83% compared to the intact vehicle control, and changes for AX (250 mg/kg) and AJ (400, 200, and 100 mg/kg) were 30.50%, 23.80%, 28.32%, and 15.51%, respectively, compared to the $PM_{2.5}$ control.

3.4. Changes in Gross Inspections and Lung Weights

Noticeable lung focal congestion and enlargement were observed in the $PM_{2.5}$ control mice compared to the intact vehicle control during gross inspections, with significant increases ($p < 0.01$) in gross congestional regions (%), lung absolute, and relative weights. However, significant reductions ($p < 0.01$) in these parameters were noted in all groups administered different dosages of AJ (400, 200, and 100 mg/kg) compared to the $PM_{2.5}$

control. AJ at a dose of 400 mg/kg demonstrated favorable inhibitory effects against lung congestion induced by $PM_{2.5}$, enlargement, and related weight increases, comparable to AX (250 mg/kg; Figure 4; Table 1). The $PM_{2.5}$ control showed a 1597.88% increase in the areas of gross congestion compared to the intact vehicle control, with changes for AX (250 mg/kg) and AJ (400, 200, and 100 mg/kg) being −61.82%, −63.90%, −46.09%, and −34.57%, respectively. Absolute lung weights in the $PM_{2.5}$ control varied by 43.59% compared to the intact vehicle control, while changes for AX (250 mg/kg) and AJ (400, 200, and 100 mg/kg) were −16.01%, −17.44%, −12.08%, and −10.30%, respectively. Relative lung weights in the $PM_{2.5}$ control changed by 44.24% compared to the intact vehicle control, with variations for AX (250 mg/kg) and AJ (400, 200, and 100 mg/kg) being −15.77%, −17.19%, −12.12%, and −10.92%, respectively.

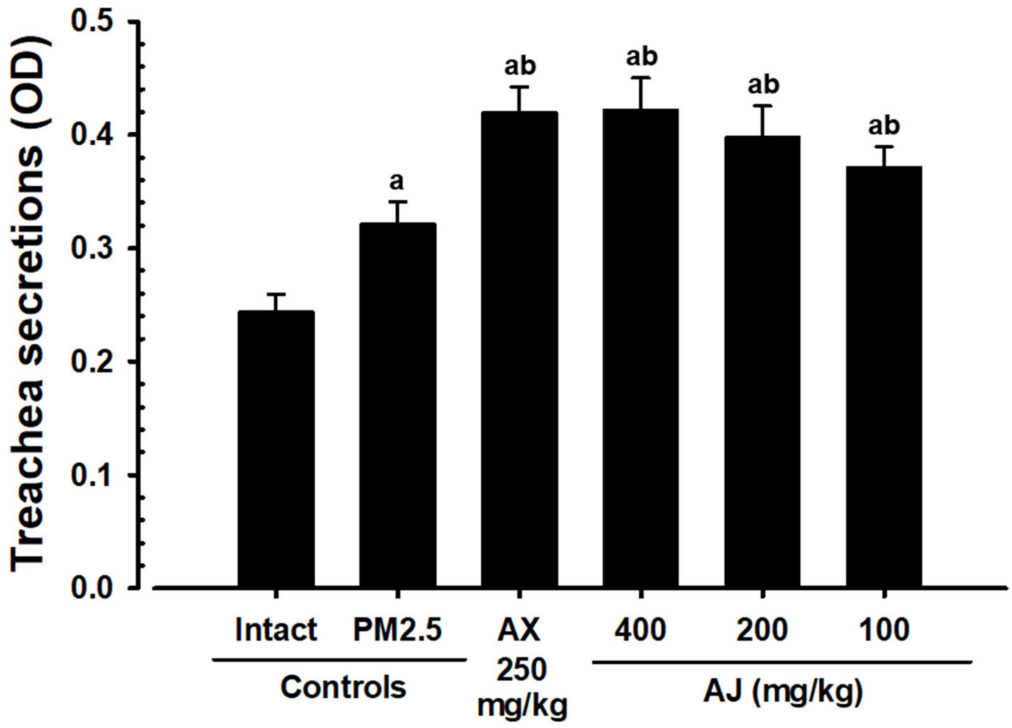


Figure 1. Tracheal pH-sensitive phenol red secretions in intact and $PM_{2.5}$-treated mice with pulmonary injury. Values are presented as means ± S.D. of 10 mice. $PM_{2.5}$ refers to diesel particulate matter NIST 1650b; AX stands for ambroxol hydrochloride, and AJ denotes Atractylodis Rhizoma (root of *Atractylodes japonica* Koidz. ex. Kitam) extracts; OD indicates optical density; THSD is Tukey's Honest Significant Difference Test. Statistical significance is indicated as follows: [a] $p < 0.01$ compared with intact vehicle control by THSD test; [b] $p < 0.01$ compared with $PM_{2.5}$ control by THSD test.

3.5. Impact on Body Surface Redness

Significant decreases ($p < 0.01$) in body surface redness were noticed in the $PM_{2.5}$ control mice compared to the intact vehicle control, suggesting respiratory distress-related blood CO_2 increase and respiratory acidosis (decrease in pH) [44]. However, significant elevations ($p < 0.01$) in body redness were noted in all dosages of AJ (400, 200, and 100 mg/kg) groups compared to the $PM_{2.5}$ control. AJ (400 mg/kg) displayed favorable inhibitory effects against $PM_{2.5}$-induced decreases in body surface redness, comparable to AX (250 mg/kg; Figures 2 and 3). The body surface redness in the $PM_{2.5}$ control varied by −68.83% compared to the intact vehicle control, while changes for AX (250 mg/kg) and AJ (400, 200, and 100 mg/kg) were 108.97%, 113.46%, 89.42%, and 65.38%, respectively, compared to the $PM_{2.5}$ control.

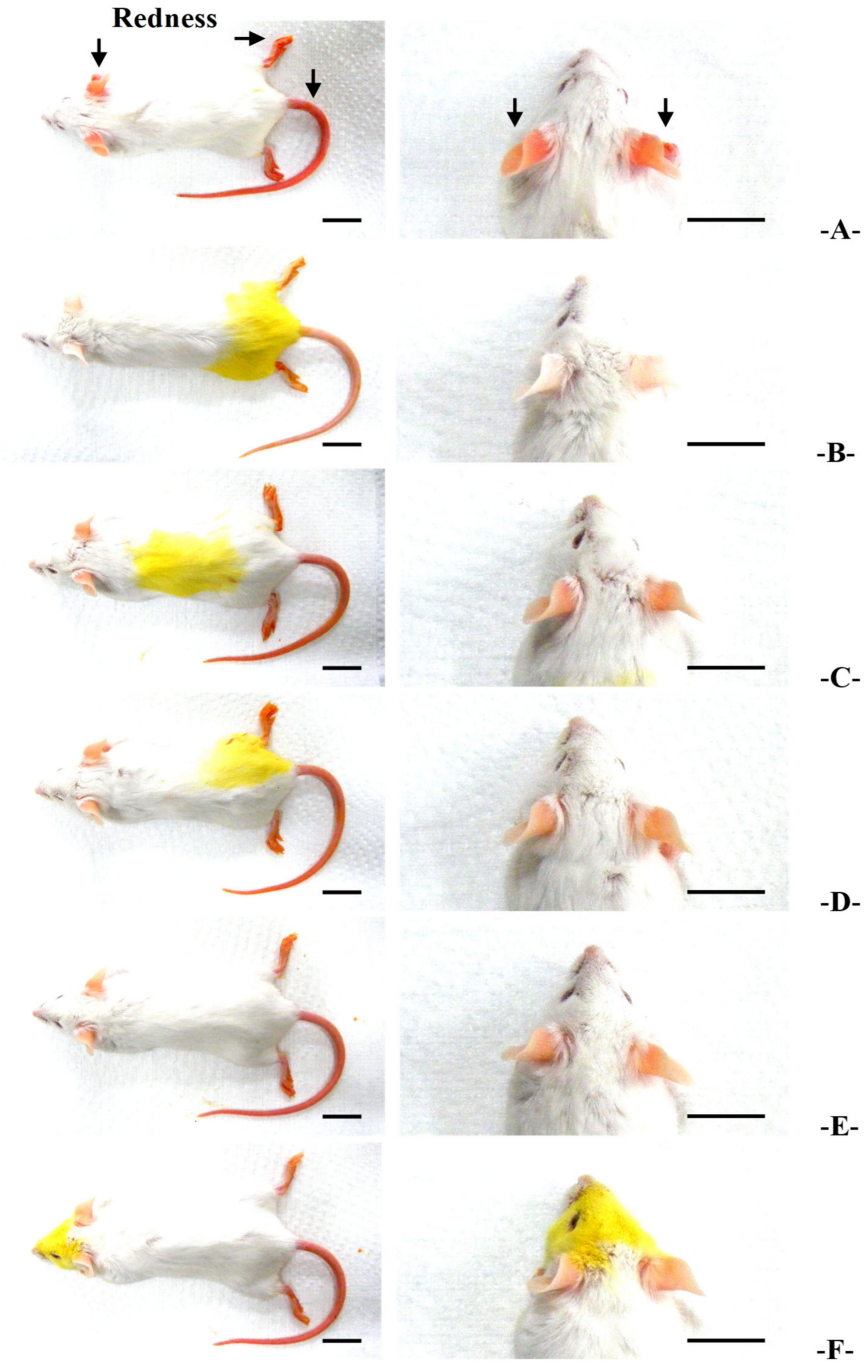


Figure 2. Illustrative images of gross skin surface from intact control and $PM_{2.5}$-treated mice with pulmonary injury. (**A**): Intact vehicle control (mice orally administered with distilled water and given saline intranasal instillation); (**B**): $PM_{2.5}$ control (mice orally administered with distilled water and given $PM_{2.5}$ intranasal instillation); (**C**): AX_{250} (mice orally administered with 250 mg/kg of AX and given $PM_{2.5}$ intranasal instillation); (**D**): AJ_{400} (mice orally administered with 400 mg/kg of AJ and given $PM_{2.5}$ intranasal instillation); (**E**): AJ_{200} (mice orally administered with 200 mg/kg of AJ and given with $PM_{2.5}$ intranasal instillation); (**F**): AJ_{100} (mice orally administered 100 mg/kg of AJ and given $PM_{2.5}$ intranasal instillation). $PM_{2.5}$ refers to diesel particulate matter NIST 1650b; AX denotes ambroxol hydrochloride; AJ stands for Atractylodis Rhizoma (root of *Atractylodes japonica* Koidz. ex. Kitam) extracts. Arrows highlight areas of congestion. Scale bars = 13.00 mm.

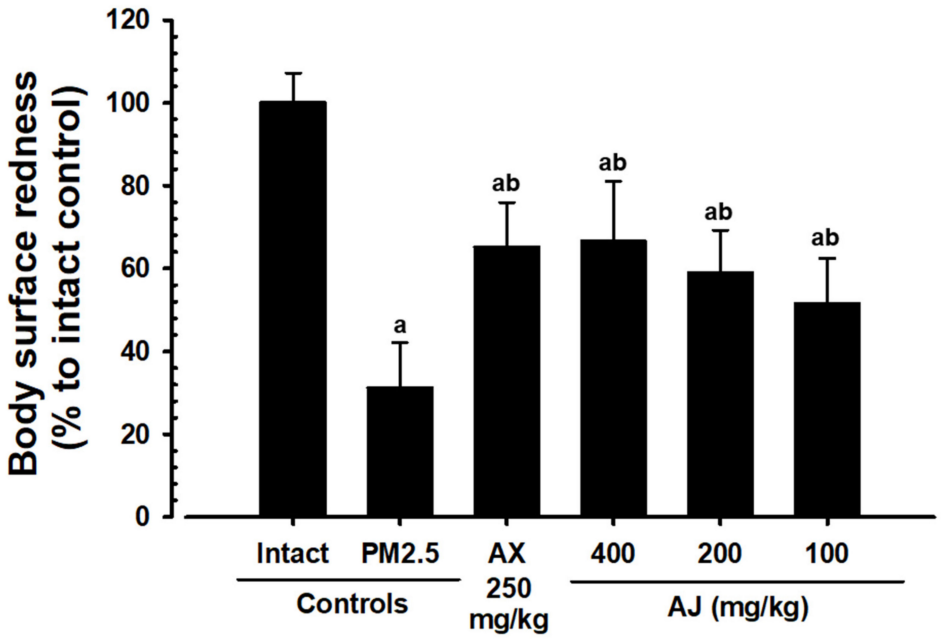


Figure 3. Body surface redness in intact control and $PM_{2.5}$-treated mice with pulmonary injury. Values are presented as means ± S.D. of 10 mice. $PM_{2.5}$ refers to diesel particulate matter NIST 1650b; AX stands for ambroxol hydrochloride, and AJ denotes Atractylodis Rhizoma (root of *Atractylodes japonica* Koidz. ex. Kitam) extracts; THSD is Tukey's Honest Significant Difference Test. Statistical significance is indicated as follows: [a] $p < 0.01$ compared with intact vehicle control by THSD test; [b] $p < 0.01$ compared with $PM_{2.5}$ control by THSD test.

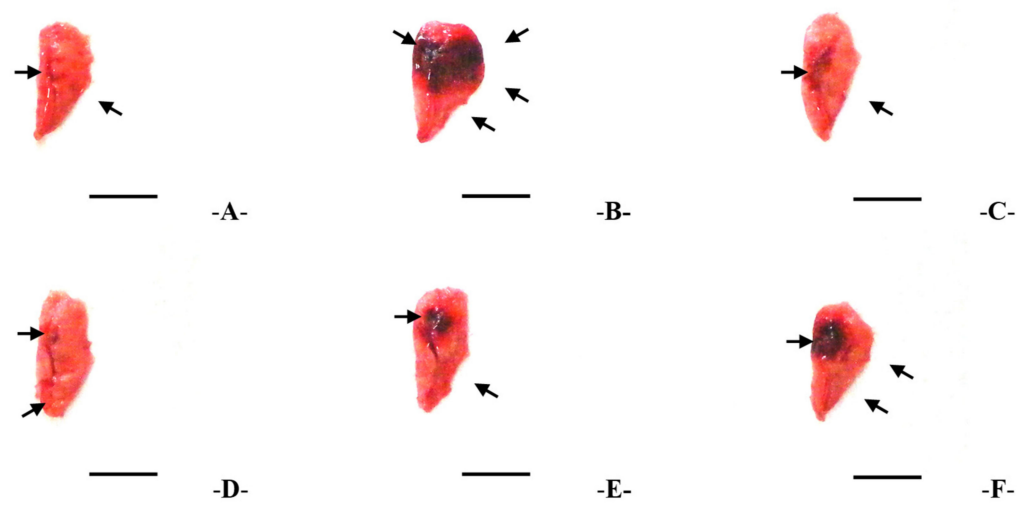


Figure 4. Illustrative images of the gross lung (left lobe) from intact control and $PM_{2.5}$-treated mice with pulmonary injury. (**A**): Intact vehicle control (mice orally administered with distilled water and given saline intranasal instillation); (**B**): $PM_{2.5}$ control (mice orally administered with distilled water and given $PM_{2.5}$ intranasal instillation); (**C**): AX_{250} (mice orally administered with 250 mg/kg of AX and given $PM_{2.5}$ intranasal instillation); (**D**): AJ_{400} (mice orally administered with 400 mg/kg of AJ and given $PM_{2.5}$ intranasal instillation); (**E**): AJ_{200} (mice orally administered with 200 mg/kg of AJ and given $PM_{2.5}$ intranasal instillation); (**F**): AJ_{100} (mice orally administered with 100 mg/kg of AJ and given $PM_{2.5}$ intranasal instillation). $PM_{2.5}$ refers to diesel particulate matter NIST 1650b; AX denotes ambroxol hydrochloride; AJ stands for Atractylodis Rhizoma (root of *Atractylodes japonica* Koidz. ex. Kitam) extracts. Arrows indicate areas of congestion. Scale bars = 6.00 mm.

Table 1. Lung mass and visual assessments in mice with pulmonary injuries, either untreated or exposed to $PM_{2.5}$.

Groups	Lung Weights		Congestional Regions (%)—Gross Findings
	Absolute (g)	Relative (%)	
Controls			
Intact vehicle	0.117 ± 0.006	0.574 ± 0.045	3.54 ± 2.66
$PM_{2.5}$	0.168 ± 0.005 [a]	0.828 ± 0.036 [a]	60.05 ± 11.37 [c]
Reference—AX			
250 mg/kg	0.141 ± 0.007 [ab]	0.698 ± 0.047 [ab]	22.93 ± 7.61 [cd]
Test substance—AJ			
400 mg/kg	0.139 ± 0.009 [ab]	0.686 ± 0.036 [ab]	21.68 ± 7.37 [cd]
200 mg/kg	0.148 ± 0.006 [ab]	0.728 ± 0.029 [ab]	32.37 ± 5.93 [cd]
100 mg/kg	0.151 ± 0.007 [ab]	0.738 ± 0.054 [ab]	39.29 ± 5.16 [cd]

Values are presented as means ± S.D. of 10 mice. $PM_{2.5}$ refers to diesel particulate matter NIST 1650b; AX denotes ambroxol hydrochloride; AJ stands for Atractylodis Rhizoma (root of *Atractylodes japonica* Koidz. ex. Kitam) extracts; THSD is Tukey's Honest Significant Difference test; DT3 is Dunnett's T3 test. Statistical significance is indicated as follows: [a] $p < 0.01$ compared with intact vehicle control by THSD test; [b] $p < 0.01$ compared with $PM_{2.5}$ control by THSD test; [c] $p < 0.01$ compared with intact vehicle control by DT3 test; [d] $p < 0.01$ compared with $PM_{2.5}$ control by DT3 test.

3.6. ACh and Substance P Levels in Lung Tissue

The $PM_{2.5}$ control mice exhibited significant increases ($p < 0.01$) in lung tissue levels of ACh and substance P compared to the intact vehicle control. In all groups administered AJ at doses of 400, 200, and 100 mg/kg, there were significant and dose-dependent elevations in these levels relative to the $PM_{2.5}$ control. AJ (400 mg/kg) exhibited favorable elevations in levels of lung tissue ACh and substance P in $PM_{2.5}$-induced subacute lung-damaged mice, comparable to AX (250 mg/kg; Figure 5). Lung tissue substance P content in the $PM_{2.5}$ control varied by 124.55% relative to the intact vehicle control, with changes for AX (250 mg/kg) and AJ (400, 200, and 100 mg/kg) being 137.62%, 143.31%, 84.10%, and 59.81%, respectively. Lung tissue ACh content in the $PM_{2.5}$ control changed by 116.24% relative to the intact vehicle control, with changes for AX (250 mg/kg) and AJ (400, 200, and 100 mg/kg) being 141.61%, 114.84%, 117.71%, 68.81%, and 43.40%, respectively.

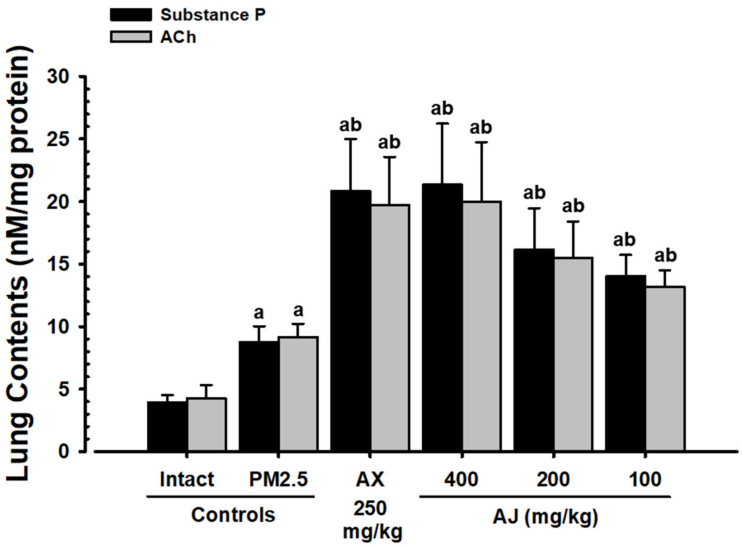


Figure 5. Lung ACh and substance P levels in mice with pulmonary injuries, either untreated or treated with $PM_{2.5}$. Values are presented as means ± S.D. of 10 mice. $PM_{2.5}$ refers to diesel particulate matter NIST 1650b; AX denotes ambroxol hydrochloride; AJ represents Atractylodis Rhizoma (root of *Atractylodes japonica* Koidz. ex. Kitam) extracts; Ach stands for acetylcholine; DT3 is Dunnett's T3 Test. Statistical significance is indicated as follows: [a] $p < 0.01$ compared with intact vehicle control by DT3 test; [b] $p < 0.01$ compared with $PM_{2.5}$ control by DT3 test.

3.7. mRNA Expressions of Genes Involved in Mucus Production

The $PM_{2.5}$ control mice exhibited significant increases ($p < 0.01$) in mRNA expressions of MUC5AC and MUC5B, which are associated with mucus production, relative to the intact control. Oral supply of AJ at doses of 400, 200, and 100 mg/kg significantly ($p < 0.01$) decreased the $PM_{2.5}$-induced elevations in a dose-dependent manner relative to the $PM_{2.5}$ control. AJ (400 mg/kg) exhibited promising inhibitory properties against $PM_{2.5}$-induced upregulation of these genes, comparable to AX (250 mg/kg; Figure 6). MUC5AC mRNA expression in the $PM_{2.5}$ control increased by 477.29% relative to the intact vehicle control, with changes for AX (250 mg/kg) and AJ (400, 200, and 100 mg/kg) being −48.96%, −52.94%, −38.41%, and −29.94%, respectively. MUC5B mRNA expression in the $PM_{2.5}$ control increased by 189.01% relative to the intact vehicle control, with changes for AX (250 mg/kg) and AJ (400, 200, and 100 mg/kg) being −36.61%, −37.19%, −28.03%, and −21.05%, respectively.

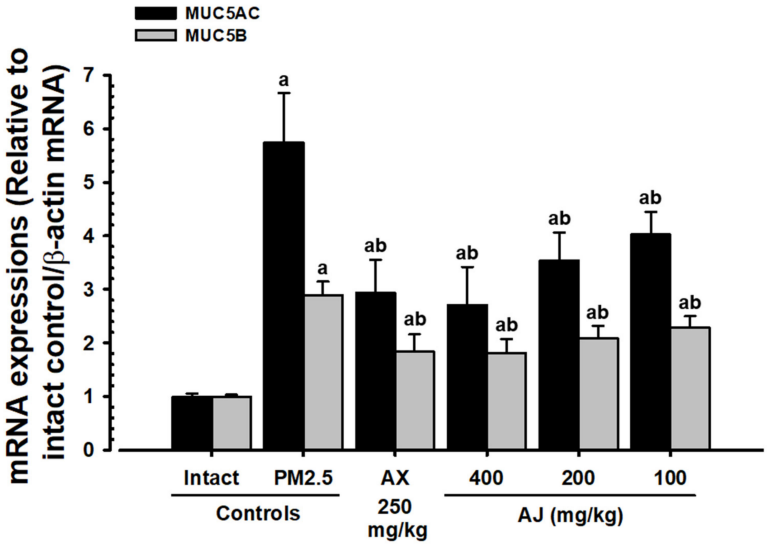


Figure 6. MUC5AC and MUC5B mRNA expression levels in lung tissue of mice with pulmonary injuries, either untreated or exposed to $PM_{2.5}$. Values are presented as means ± S.D. of 10 mice. $PM_{2.5}$ refers to diesel particulate matter NIST 1650b; AX stands for ambroxol hydrochloride; AJ indicates Atractylodis Rhizoma (root of *Atractylodes japonica* Koidz. ex. Kitam) extracts; MUC represents Mucin; DT3 is Dunnett's T3 test. Statistical significance is indicated as follows: [a] $p < 0.01$ compared with intact vehicle control by DT3 test; [b] $p < 0.01$ compared with $PM_{2.5}$ control by DT3 test.

3.8. Lung Histopathological Inspections

Significant sarcomatous changes, including inflammatory cell infiltration-related thickening of the alveolar septum, thickening of secondary bronchus mucosa, and hyperplasia of PAS+ mucus-producing cells, were noticed following two 48 h interval intranasal instillations of $PM_{2.5}$ (1 mg/kg). These findings were validated through histomorphometrical analysis. The $PM_{2.5}$ control mice exhibited significant increases ($p < 0.01$) in mean alveolar septal thickness, secondary bronchus mucosa thickness, and increased numbers of PAS+ mucus-producing cells and infiltrating inflammatory cells in alveolar regions, along with decreases in ASA when compared to the untreated vehicle control mice. However, dose-dependent and significant ($p < 0.01$) improvements were observed by oral administration of AJ (400, 200, and 100 mg/kg) compared to the $PM_{2.5}$ control. AJ (400 mg/kg) showed favorable inhibitory activities against $PM_{2.5}$-induced septal thickening and inflammation, comparable to AX (250 mg/kg; Figure 7; Table 2). Mean ASA in the $PM_{2.5}$ control changed by −47.85% compared to in the intact vehicle control, with changes for AX (250 mg/kg) and AJ (400, 200, and 100 mg/kg) being 64.31%, 65.75%, 55.30%, and 45.47%, respectively.

Alveolar septal thickness in the $PM_{2.5}$ control changed by 709.96% compared to intact vehicle control, with changes for AX (250 mg/kg) and AJ (400, 200, and 100 mg/kg) being −59.93%, −61.09%, −47.81%, and −36.40%, respectively. The secondary bronchus mucosa thickness in the $PM_{2.5}$ control changed by 34.19% compared to the intact vehicle control, with changes for AX (250 mg/kg) and AJ (400, 200, and 100 mg/kg) being 41.48%, 45.20%, 32.06%, and 18.44%, respectively. Inflammatory cell infiltration in the $PM_{2.5}$ control altered by 756.75% compared to the intact vehicle control, with changes for AX (250 mg/kg) and AJ (400, 200, and 100 mg/kg) being −63.34%, −64.71%, −53.22%, and −38.49%, respectively. PAS+ mucus-producing cell numbers in the $PM_{2.5}$ control changed by 71.25% compared to the intact vehicle control, with changes for AX (250 mg/kg) and AJ (400, 200, and 100 mg/kg) being 99.03%, 101.95%, 63.50%, and 37.71%, respectively.

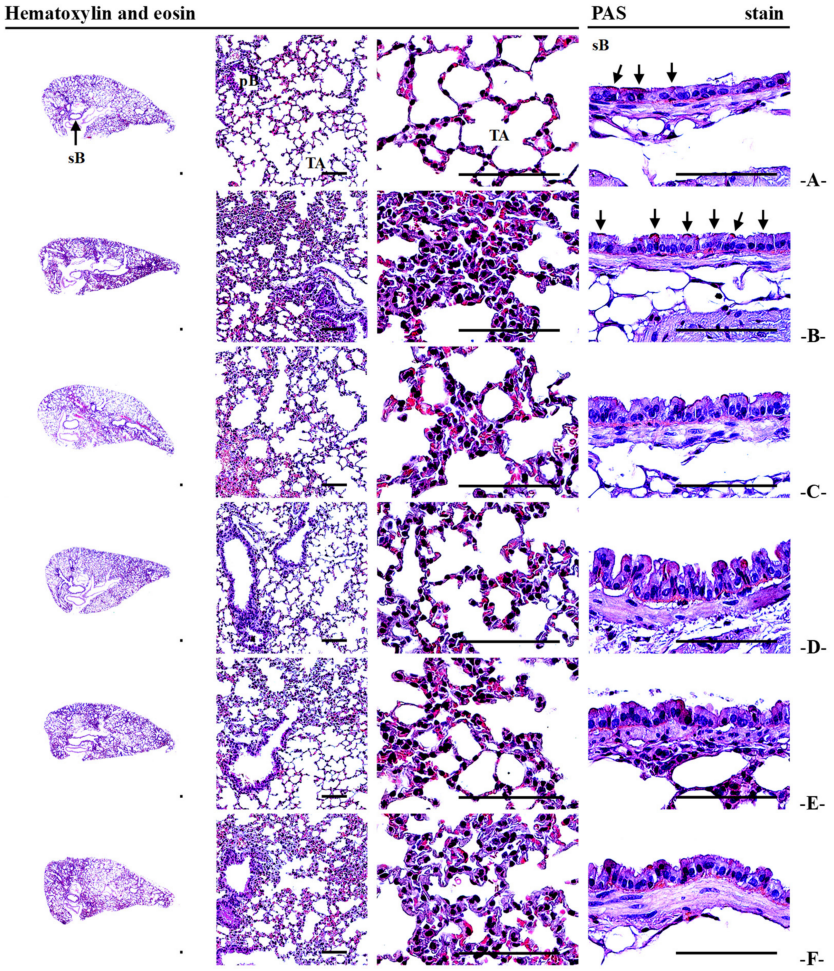


Figure 7. Illustrative histopathological profiles of the lung tissues from the left lobe of mice with pulmonary injuries, either untreated or treated with $PM_{2.5}$. (**A**): Intact vehicle control (mice orally administered with distilled water and given saline intranasal instillation); (**B**): $PM_{2.5}$ control (mice orally administered with distilled water and given $PM_{2.5}$ intranasal instillation); (**C**): AX_{250} (mice orally administered with 250 mg/kg of AX and given $PM_{2.5}$ intranasal instillation); (**D**): AJ_{400} (mice orally administered with 400 mg/kg of AJ orally and given $PM_{2.5}$ intranasal instillation); (**E**): AJ_{200} (mice orally administered with 200 mg/kg of AJ and given $PM_{2.5}$ intranasal instillation); (**F**): AJ_{100} (mice orally administered with 100 mg/kg of AJ and given $PM_{2.5}$ intranasal instillation). $PM_{2.5}$ refers to diesel particulate matter NIST 1650b; AX indicates ambroxol hydrochloride; AJ stands for Atractylodis Rhizoma (root of *Atractylodes japonica* Koidz. ex. Kitam) extracts; ASA denotes alveolar surface area; sB is secondary bronchus; PAS stands for periodic acid Schiff; pB is primary bronchiole; TA refers to terminal respiratory bronchiole-alveoli. Arrows indicate PAS+ mucus-producing cells. Scale bars = 200 μm.

Table 2. Overview of histomorphometric analysis of left lobe lung tissue in mice with pulmonary injuries, either untreated or treated with $PM_{2.5}$.

Groups	Mean ASA (%/mm^2)	Mean Alveolar Septal Thickness (μm)	Mean Thickness of SB (μm)	Mean IF Cell Numbers Infiltrated in AR (cells/mm^2)	PAS+ Cells on the SB (cells/mm^2)
Controls					
Intact vehicle	79.96 ± 10.72	5.80 ± 2.32	13.32 ± 1.47	72.60 ± 21.77	24.00 ± 3.89
$PM_{2.5}$	41.70 ± 4.34 [a]	47.01 ± 7.98 [d]	17.87 ± 1.17 [d]	622.00 ± 119.37 [d]	41.10 ± 5.47 [d]
Reference—AX					
250 mg/kg	68.51 ± 8.89 [c]	18.84 ± 4.97 [de]	25.29 ± 2.84 [de]	228.00 ± 62.21 [de]	81.80 ± 15.33 [de]
Test substance—AJ					
400 mg/kg	69.12 ± 10.86 [c]	18.29 ± 4.92 [de]	25.95 ± 3.64 [de]	219.50 ± 56.54 [de]	83.00 ± 12.73 [de]
200 mg/kg	64.76 ± 10.29 [bc]	24.53 ± 5.24 [de]	23.60 ± 2.20 [de]	291.00 ± 70.79 [de]	67.20 ± 11.44 [de]
100 mg/kg	60.66 ± 10.74 [ac]	29.90 ± 4.78 [de]	21.17 ± 0.81 [de]	382.60 ± 52.20 [de]	56.60 ± 6.11 [de]

Values are presented as means ± S.D. of 10 mice. $PM_{2.5}$ refers to diesel particulate matter NIST 1650b; AX indicates ambroxol hydrochloride; AJ stands for Atractylodis Rhizoma (root of *Atractylodes japonica* Koidz. ex. Kitam) extracts; SB is secondary bronchus mucosa; ASA denotes alveolar surface area; IF stands for inflammatory; AR is alveolar region; PAS refers to periodic acid Schiff; THSD is Tukey's Honest Significant Difference test; DT3 is Dunnett's T3 test. Statistical significance is indicated as follows: [a] $p < 0.01$ and [b] $p < 0.05$ compared with intact vehicle control by THSD test; [c] $p < 0.01$ compared with $PM_{2.5}$ control by THSD test; [d] $p < 0.01$ compared with intact vehicle control by DT3 test; [e] $p < 0.01$ compared with $PM_{2.5}$ control by DT3 test.

3.9. Lung Immunohistochemical Analysis

Significant increases ($p < 0.01$) in inflammation-related COX-2 and apoptosis-related cleaved caspase-3 immunopositive cell numbers were demonstrated in the alveolar septum and secondary bronchus mucosa regions of the $PM_{2.5}$ control mice relative to intact vehicle control. The $PM_{2.5}$-induced elevations were significantly ($p < 0.01$) and dose-dependently limited by the oral supply of AJ at doses of from 400 to 100 mg/kg, relative to the $PM_{2.5}$ control. AJ (400 mg/kg) showed promising inhibitory properties against $PM_{2.5}$-induced elevations in apoptosis and inflammation markers, comparable to AX (250 mg/kg; Figure 8; Table 3). Cleaved caspase-3 immunoreactive cells in the alveolar septum of the $PM_{2.5}$ control changed by 815.93% relative to the intact vehicle control, with changes for AX (250 mg/kg) and AJ (400, 200, and 100 mg/kg) being −66.96%, −68.07%, −54.15%, and −26.96%, respectively. Cleaved caspase-3 immunopositive cells in the secondary mucosa of the $PM_{2.5}$ control changed by 535.71% compared to the intact vehicle control, with changes for AX (250 mg/kg) and AJ (400, 200, and 100 mg/kg) being −71.24%, −71.46%, −57.87%, and −50.45%, respectively. COX-2 immunolabeled cells in the alveolar septum of the $PM_{2.5}$ control changed by 1003.70% compared to the intact vehicle control, with changes for AX (250 mg/kg) and AJ (400, 200, and 100 mg/kg) being −73.83%, −75.66%, −59.42%, and −29.84%, respectively. COX-2 immunostained cells in the secondary mucosa of the $PM_{2.5}$ control changed by 476.06% compared to the intact vehicle control, with changes for AX (250 mg/kg) and AJ (400, 200, and 100 mg/kg) being −61.59%, −66.20%, −50.69%, and −27.05%, respectively.

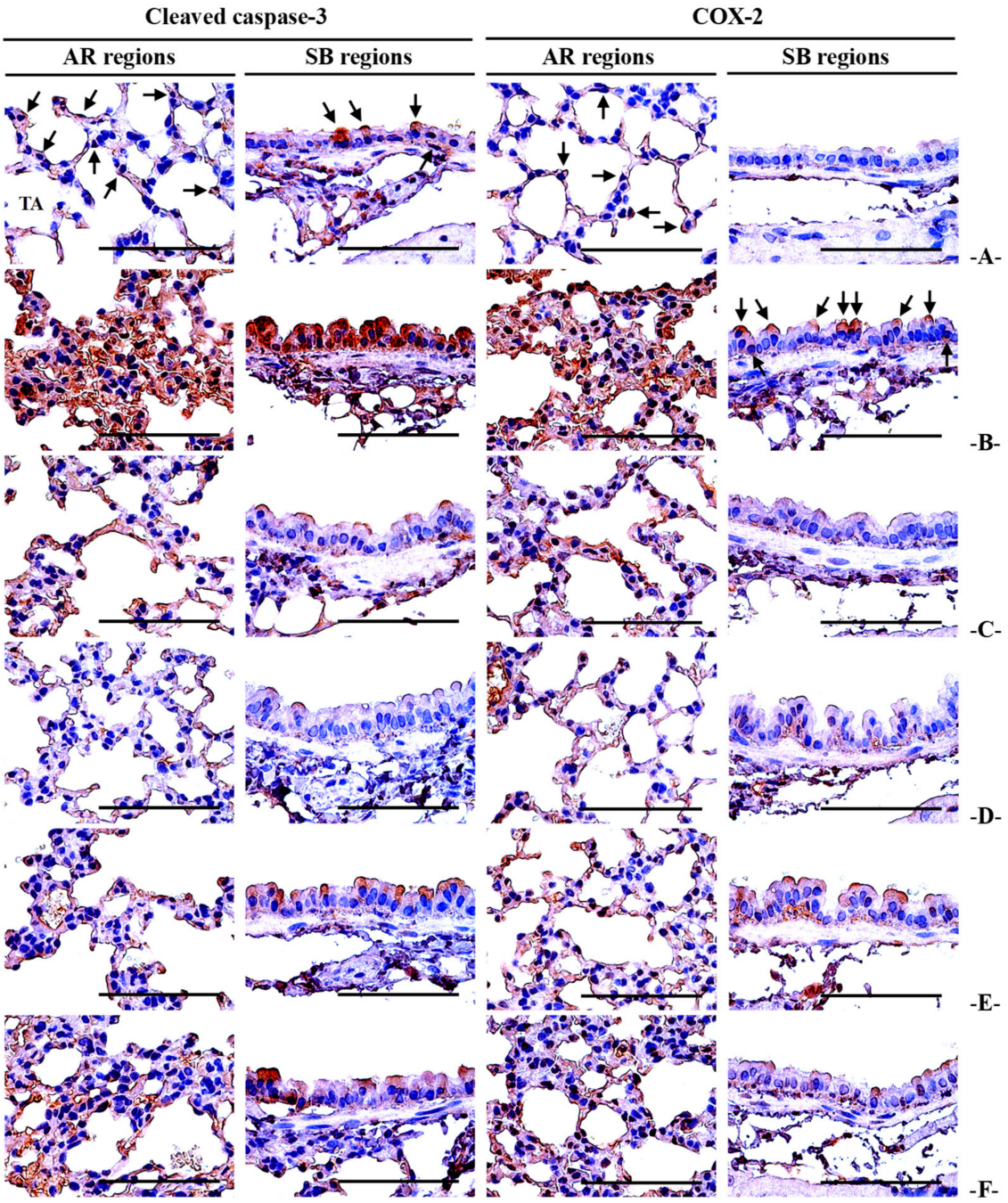


Figure 8. Illustrative profiles of lung tissue from the left lobe, based on immunohistochemistrical staining, in mice with pulmonary injuries, either untreated or treated with $PM_{2.5}$. (**A**): Intact vehicle control (mice orally administered with distilled water and given saline intranasal instillation); (**B**): $PM_{2.5}$ control (mice orally administered with distilled water and given $PM_{2.5}$ intranasal instillation); (**C**): AX_{250} (mice orally supplied with 250 mg/kg of AX and given $PM_{2.5}$ intranasal instillation); (**D**): AJ_{400} (mice orally supplied with 400 mg/kg of AJ and given $PM_{2.5}$ intranasal instillation); (**E**): AJ_{200} (mice orally supplied with 200 mg/kg of AJ and given $PM_{2.5}$ intranasal instillation); (**F**): AJ_{100} (mice orally supplied with 100 mg/kg of AJ and given $PM_{2.5}$ intranasal instillation). $PM_{2.5}$ refers to diesel particulate matter NIST 1650b; AX stands for ambroxol hydrochloride; AJ indicates Atractylodis Rhizoma (root of *Atractylodes japonica* Koidz. ex. Kitam) extracts; SB is secondary bronchus mucosa; AR denotes alveolar septal; COX stands for cyclooxygenase; ABC refers to avidin-biotin-peroxidase complex; TA stands for terminal respiratory bronchiole-alveoli. Arrows indicate immunoreactive cells. Scale bars = 200 μm.

Table 3. Histomorphometrical analysis of left lobe lung tissue in mice with pulmonary injuries, either untreated or treated with $PM_{2.5}$.

Groups	Caspase-3 Immunolabeled Cells		COX-2 Immunostained Cells	
	AR Region	SB Mucosa Region	AR Region	SB Mucosa Region
Controls				
Intact vehicle	45.20 ± 15.75	28.00 ± 6.93	40.50 ± 10.38	18.80 ± 3.55
$PM_{2.5}$	414.00 ± 57.25 [a]	178.00 ± 17.13 [c]	447.00 ± 83.60 [cd]	108.30 ± 12.33 [a]
Reference—AX				
250 mg/kg	138.80 ± 38.52 [ab]	51.20 ± 11.75 [cd]	117.00 ± 30.17 [cd]	41.60 ± 7.93 [ab]
Test substance—AJ				
400 mg/kg	132.20 ± 35.14 [ab]	50.80 ± 14.30 [cd]	108.80 ± 15.73 [cd]	36.60 ± 12.65 [ab]
200 mg/kg	189.80 ± 62.07 [ab]	75.00 ± 17.62 [cd]	181.40 ± 81.49 [cd]	53.40 ± 13.23 [ab]
100 mg/kg	302.40 ± 37.14 [ab]	88.20 ± 25.90 [cd]	313.60 ± 23.79 [cd]	79.00 ± 10.03 [ab]

Values are presented as means ± S.D. of 10 mice, measured in cells/mm^2. $PM_{2.5}$ refers to diesel particulate matter NIST 1650b; AX denotes ambroxol hydrochloride; AJ indicates Atractylodis Rhizoma (root of *Atractylodes japonica* Koidz. ex. Kitam) extracts; COX stands for cyclooxygenase; SB represents secondary bronchus mucosa; AR is alveolar septal; THSD is Tukey's Honest Significant Difference test; DT3 is Dunnett's T3 test. Statistical significance is indicated as follows: [a] $p < 0.01$ compared with intact vehicle control by THSD test; [b] $p < 0.01$ compared with $PM_{2.5}$ control by THSD test; [c] $p < 0.01$ compared with intact vehicle control by DT3 test; [d] $p < 0.01$ compared with $PM_{2.5}$ control by DT3 test.

4. Discussion

During the ten-day experimental period, no notable variations in body weight or weight gains were noticed in the $PM_{2.5}$ intranasally instilled mice compared to the intact vehicle control mice. Similarly, mice administered orally with AJ (400–100 mg/kg), as well as those given the reference drug, AX (250 mg/kg), showed no significant differences in body weight or weight gains relative to the $PM_{2.5}$ control. Each group, including the intact vehicle, the $PM_{2.5}$ control, and the AX- and AJ-administered mice, exhibited normal weight increases consistently with age-matched mice of the same strain [45].

Expectorants function by prompting the body to increase secretion volume or hydration, resulting in clearer secretions that help lubricate the respiratory tract. This mechanism is beneficial for alleviating various respiratory disorders [14,15]. The expectorant effects of the drugs were evaluated by examining their ability to induce mucus secretion using the pH-sensitive dye phenol red in a tracheal secretion technique in mice [15–19]. Thirty minutes after a single intraperitoneal injection of a 5% phenol red solution, the $PM_{2.5}$ control group exhibited significantly higher tracheal phenol red secretions compared to the intact control. Furthermore, noteworthy and dose-dependent increases in phenol red secretions were noted in groups administered AJ from 400 to 100 mg/kg, relative to the $PM_{2.5}$ control. The group receiving 400 mg/kg of AJ revealed especially promising increases in phenol red secretions comparable to the AX (250 mg/kg) group in the $PM_{2.5}$-induced subacute lung-damaged mice. Phenol red is a pH-sensitive dye that transitions in color from yellow to red as the pH rises. It serves as an important pH indicator in biological tissues [44,46]. Since reductions in blood pH, indicative of respiratory acidosis, are associated with increased CO_2 levels and H_2CO_3 formation, the decreased body surface redness observed in the $PM_{2.5}$ control mice may serve as indirect evidence of respiratory acidosis due to $PM_{2.5}$ inhalation [47,48]. However, AJ treatment led to significant, dose-dependent increases in body redness, suggesting inhibition of $PM_{2.5}$-induced acidosis. AJ at 400 mg/kg showed a particularly favorable inhibition of body surface redness comparable to AX at 250 mg/kg. These findings provide an indirect but consistent indication that AJ from 400 to 100 mg/kg exhibits potent suppressive effects on $PM_{2.5}$-induced respiratory acidosis, potentially through mucolytic expectorant activities.

Respiratory mucus serves as a defensive barrier against foreign particles and pathogens [49,50]. Mucins, which are glycoprotein components, define the viscoelastic char-

acteristics of mucus, which is essential for effective mucociliary clearance [51]. MUC5AC and MUC5B are the primary secretory mucins involved [49,50]. Studies indicate that $PM_{2.5}$ induces the overexpression of these mucins, enhancing mucus production [49,50,52]. Neural control, via acetylcholine (ACh) and substance P, regulates serous gland secretions [49]. Substance P functions as a mediator in neurogenic inflammation, and its levels increase with $PM_{2.5}$ exposure in the airways [53–55]. Similarly, ACh levels increase with $PM_{2.5}$ exposure, functioning as a vascular relaxant related to inflammatory vascular permeability, although the vascular response to ACh is impaired in $PM_{2.5}$-treated mice [2,3,56,57]. Consistent with previous findings, the levels of lung tissue serous secretagogues, Ach, and substance P were significantly elevated after a 10-day continuous oral supply of AJ (400–100 mg/kg). This increase corresponded with significant and dose-dependent reductions in the mRNA expressions of mucus production-related genes, MUC5B and MUC5AC, relative to the $PM_{2.5}$ control. These findings were comparable to those seen with AX at 250 mg/kg. This suggests potent mucolytic expectorant activities, possibly through increased secretion of substance P and ACh, leading to serous secretagogue effects and suppression of MUC5AC and MUC5B mRNA expressions, resulting in decreased mucin production under the conditions of the current analysis. AJ administration significantly reduced the expressions of MUC5AC and MUC5B mRNA, indicating potent mucolytic expectorant effects through increased secretion of ACh and substance P [54,55]. ACh and substance P are the primary neurotransmitters involved in serous secretions, acting as serous secretagogues, particularly in goblet cells and acinar cells in the respiratory system. Therefore, the increases in ACh and substance P due to AJ and AX may have been induced by serous secretions and the dilution of mucous, which is elevated by $PM_{2.5}$ exposure. It can be regarded as another possible mechanism for their expectorant activities.

The lung weight index, defined as the proportion of lung weight to body weight, is commonly regarded both generally and biochemically as a reliable indicator of vascular permeability and edema [37,58]. Similar to the ovalbumin-induced asthmatic mouse model [59], mice exposed to $PM_{2.5}$ through instillation methods demonstrated increased microvascular leakage, leading to heightened lung congestion and edema [2,3]. In the present study, noticeable lung focal congestion with enlargement was also observed in the $PM_{2.5}$ control mice relative to the intact vehicle control upon gross inspection. Remarkable increases in gross congestional regions (%), as well as lung relative and absolute weights, were observed in the $PM_{2.5}$ control relative to the intact vehicle controls. However, noticeable decreases in gross congestional regions (%) and lung absolute and relative weights were noticed in all AJ (400–100 mg/kg)-supplied mice in a dose-dependent manner. Notably, mice treated with 400 mg/kg of AJ exhibited beneficial inhibitory effects on $PM_{2.5}$-induced lung congestion, enlargement, and the corresponding increases in both absolute and relative lung weights, similar to the effects seen with 250 mg/kg of AX. These findings suggest that the oral supply of AJ from 400 to 100 mg/kg effectively inhibited the $PM_{2.5}$-induced lung congestive edema and the associated elevations in lung index relative to the impact of AX at 250 mg/kg. The effects were particularly pronounced in the AJ (400 mg/kg) group, indicating a dose-dependent response, potentially via promising mucolytic, expectorant, or anti-inflammatory effects.

The histomorphometric index, ASA (%/mm^2), is indicative of pulmonary function and gas exchange capacity, with decreases suggesting reduced lung surface area and capacity, which are commonly seen in various lung diseases [18,19,24,37,60]. PAS staining identifies mucous-producing cells, with a higher intensity indicating greater activity [18,19,61] and increased bronchial mucosa thickness, and PAS+ cells associated with expectorant effects [16–19]. Apoptosis, a regulated process causing cell death, is marked by chromatin condensation and apoptosis, with cleaved caspase-3 as a key executioner [62]. $PM_{2.5}$ expo-

sure increases cleaved caspase-3 in lung tissue, indicating apoptosis and damage [63,64], while oxidative stress from $PM_{2.5}$ interrupts the oxidative defense system and mediates mitochondria-dependent apoptosis [65]. COX-2, an enzyme crucial for prostaglandin synthesis and inflammation, is also involved in lung damage induced by $PM_{2.5}$ [66,67]. Decreased COX-2 immunoreactivity signals the beneficial effects of treatments on inflammation [68,69]. In mice, $PM_{2.5}$-induced pulmonary injuries include inflammatory cell infiltration and alveolar septum thickening [2,3,70,71], with histopathological observations showing hyperplasia of PAS+ mucus-producing cells, decreased ASA, increased bronchial mucosa thickness, and elevated cleaved COX-2 and caspase-3 activity after $PM_{2.5}$ exposure. Oral supply of AJ (400–100 mg/kg) increased ASA and decreased septal thickness, inflammatory infiltration, and apoptosis markers in a dose-dependent manner, with AJ at 400 mg/kg showing effects comparable to AX at 250 mg/kg. AJ also increased PAS+ cell numbers and bronchial mucosa thickness, indicating potent expectorant activity [16]. These findings indicate that AJ offers substantial pulmonary protection against $PM_{2.5}$-induced injuries through its anti-inflammatory and mucolytic properties, supporting its potential as a candidate for respiratory health products. These results align with previous studies demonstrating AJ's protective effects against human diseases [23,32,33]. Consequently, appropriate oral administration of AJ could serve as a viable candidate for developing alternative respiratory refinement agents or functional food ingredients, backed by its dose-dependent protective effects in $PM_{2.5}$-induced pulmonary injury models.

This study explored the dose-dependent expectorant activities of AJ, which consistently demonstrated promising results. The effects observed may be linked to bioactive compounds, atractylenolide I and III, found in the roots of *A. japonica*. These compounds have been pharmacologically validated for their expectorant, anti-inflammatory, anti-allergic, anti-cancer, gastroprotective, and assimilation-enhancing properties [72–76]. However, under the conditions of the current experiment, it is challenging to conclude whether the expectorant activity of AJ at 400 mg/kg represents a threshold effect or is influenced by the compound's bioavailability. To address these limitations, future studies should involve detailed mechanism studies, expanded dosage range investigations, and efficacy studies in long-term $PM_{2.5}$ exposure or other animal models, such as asthma. This approach, coupled with screening of bioactive compounds, is essential before drawing definitive conclusions.

5. Conclusions

This study evaluated critical parameters related to the expectorant effects on $PM_{2.5}$-induced sub-acute pulmonary injuries in Balb/c mice. The results exhibited that oral administration of AJ from 400 to 100 mg/kg provides significant pulmonary protective effects against $PM_{2.5}$-induced damage, excessive mucus production, and respiratory acidosis. These protective effects are likely due to AJ's strong anti-inflammatory and mucolytic expectorant activities, as evidenced by elevated levels of lung ACh and substance P, along with the suppression of MUC5B and MUC5AC mRNA expressions. The impact of AJ at 400 mg/kg was similar to that of AX (250 mg/kg) under the experimental conditions. Exposure to $PM_{2.5}$ resulted in increased phenol red secretions, lung congestion, elevated levels of ACh, and substance P, and the upregulation of mucus production genes, leading to inflammatory lung injuries and respiratory acidosis. However, these negative effects were significantly and dose-dependently mitigated by a 10-day AJ administration. Notably, AJ at 400 mg/kg exhibited effective inhibition of pulmonary injuries, similar to AX at 250 mg/kg, via anti-inflammatory pathways. Additionally, the AJ administration led to increased phenol red secretions, higher PAS+ cell counts, and thicker bronchial mucosa, with reduced MUC5AC and MUC5B expression, indicating potent mucolytic expectorant activity. These findings highlight the possibility that AJ may be a promising candidate for

developing alternative respiratory health products or functional food ingredients, based on its demonstrated dose-dependent pulmonary protective properties.

Supplementary Materials: The following supporting information can be downloaded at https://www.mdpi.com/article/10.3390/app15010099/s1: Table S1. Specific conditions for HPLC analysis; Table S2. Oligonucleotides used for quantitative RT-PCR; Table S3. Primary antisera and detection kits used for immunohistochemistry; Figure S1. HPLC chromatogram of atractylenolide III in *Atractylodes japonica* root extract; Figure S2. Changes in body weights of intact or $PM_{2.5}$-treated mice with pulmonary injury.

Author Contributions: Conceptualization, Y.-S.K. and S.-K.K.; methodology, J.L. (Junho Lee), J.L. (Jeongjun Lee), H.C., Y.-S.K. and S.-K.K.; software, S.-K.K.; validation, Y.-S.K., K.M.I.B., J.-S.C. and S.-K.K.; formal analysis, J.L. (Junho Lee), S.M., Y.-S.K. and S.-K.K.; investigation, Y.-S.K. and S.-K.K.; resources, S.-K.K.; data curation, J.L. (Junho Lee), S.M., J.L. (Jeongjun Lee) and H.C.; writing—original draft preparation, J.L. (Junho Lee), S.M. and K.M.I.B.; writing—review and editing, S.M., Y.-S.K., K.M.I.B., J.-S.C. and S.-K.K.; visualization, Y.-S.K., K.M.I.B., J.-S.C. and S.-K.K.; supervision, Y.-S.K., J.-S.C. and S.-K.K.; project administration, S.-K.K.; funding acquisition, S.-K.K. All authors have read and agreed to the published version of the manuscript.

Funding: This work was supported by a research grant from the Gyeongsang National University in 2024.

Institutional Review Board Statement: The animal study was approved by the Animal Experimentation Ethics Committee of Daegu Haany University [Approval No.: DHU2022-016; Approved on: 22 February 2022].

Informed Consent Statement: Not applicable.

Data Availability Statement: The original contributions presented in this study are contained within the article and Supplementary Materials; further inquiries can be directed to the corresponding authors.

Conflicts of Interest: Authors Jeongjun Lee and Hunsuk Chung were employed by the company GAPI BIO Co., Ltd., Republic of Korea. The remaining authors declare that the research was conducted in the absence of any commercial or financial relationships that could be construed as a potential conflict of interest.

References

1. Fernando, I.P.S.; Jayawardena, T.U.; Kim, H.S.; Lee, W.W.; Vaas, A.P.J.P.; De Silva, H.I.C.; Abayaweera, G.S.; Nanayakkara, C.M.; Abeytunga, D.T.U.; Lee, D.S.; et al. Beijing urban particulate matter-induced injury and inflammation in human lung epithelial cells and the protective effects of fucosterol from *Sargassum binderi* (Sonder ex J. Agardh). *Environ. Res.* **2019**, *172*, 150–158. [CrossRef] [PubMed]
2. Lee, W.; Ku, S.-K.; Kim, J.E.; Cho, S.H.; Song, G.Y.; Bae, J.S. Inhibitory effects of protopanaxatriol type ginsenoside fraction (Rgx365) on particulate matter-induced pulmonary injury. *J. Toxicol. Environ. Health A* **2019**, *82*, 338–350. [CrossRef] [PubMed]
3. Lee, W.; Ku, S.-K.; Kim, J.E.; Cho, S.H.; Song, G.Y.; Bae, J.S. Inhibitory effects of black ginseng on particulate matter-induced pulmonary injury. *Am. J. Chin. Med.* **2019**, *47*, 1237–1251. [CrossRef] [PubMed]
4. Zhuang, G.; Guo, J.; Yuan, H.; Zhao, C. The compositions, sources, and size distribution of the dust storm from China in spring of 2000 and its impact on the global environment. *Chin. Sci. Bull.* **2001**, *46*, 895–900. [CrossRef]
5. Wang, W.; Primbs, T.; Tao, S.; Simonich, S.L. Atmospheric particulate matter pollution during the 2008 Beijing Olympics. *Environ. Sci. Technol.* **2009**, *43*, 5314–5320. [CrossRef]
6. Huang, X.F.; He, L.Y.; Hu, M.; Zhang, Y.H. Annual variation of particulate organic compounds in PM2.5 in the urban atmosphere of Beijing. *Atmos. Environ.* **2006**, *40*, 2449–2458. [CrossRef]
7. Zhang, Y.; Tian, J.; Wang, Q.; Qi, L.; Manousakas, M.I.; Han, Y.; Ran, W.; Sun, Y.; Liu, H.; Zhang, R.; et al. High-time-resolution chemical composition and source apportionment of PM2.5 in northern Chinese cities: Implications for policy. *Atmos. Chem. Phys.* **2023**, *23*, 9455–9471. [CrossRef]
8. Zhang, J.; Su, Y.; Chen, C.; Guo, W.; Tan, Q.; Feng, M.; Song, D.; Jiang, T.; Chen, Q.; Li, Y.; et al. Chemical composition, sources and formation mechanism of urban PM2.5 in Southwest China: A case study at the beginning of 2023. *Atmos. Chem. Phys.* **2024**, *24*, 2803–2820. [CrossRef]

9. Chiu, H.F.; Tsai, S.S.; Yang, C.Y. Short-term effects of fine particulate air pollution on hospital admissions for hypertension: A time-stratified case-crossover study in Taipei. *J. Toxicol. Environ. Health A* **2017**, *80*, 258–265. [CrossRef]
10. Nunes, C.; Pereira, A.M.; Morais-Almeida, M. Asthma costs and social impact. *Asthma Res. Pract.* **2017**, *3*, 1. [CrossRef]
11. Schaumann, F.; Borm, P.J.; Herbrich, A.; Knoch, J.; Pitz, M.; Schins, R.P.; Luettig, B.; Hohlfeld, J.M.; Heinrich, J.; Krug, N. Metal-rich ambient particles (particulate matter 2.5) cause airway inflammation in healthy subjects. *Am. J. Respir. Crit. Care Med.* **2004**, *170*, 898–903. [CrossRef] [PubMed]
12. Birring, S.S.; Prudon, B.; Carr, A.J.; Singh, S.J.; Morgan, M.D.; Pavord, I.D. Development of a symptom specific health status measure for patients with chronic cough. *Leic. Cough Quest. (LCQ) Thorax* **2003**, *58*, 339–343.
13. Dicpinigaitis, P.V.; Gayle, Y.E. Effect of guaifenesin on cough reflex sensitivity. *Chest* **2003**, *124*, 2178–2181. [CrossRef] [PubMed]
14. Garay, A.G.G.; Reveiz, L.; Hidalgo, L.V.; Galicia, C.S. Ambroxol for women at risk of preterm birth for preventing neonatal respiratory distress syndrome. *Cochrane Database Syst. Rev.* **2014**, *2014*, CD009708.
15. Rubin, B.K. Aerosol medications for treatment of mucus clearance disorders. *Respir. Care.* **2015**, *60*, 825–829. [CrossRef]
16. Wang, D.; Wang, S.; Chen, X.; Xu, X.; Zhu, J.; Nie, L.; Long, X. Antitussive, expectorant and anti-inflammatory activities of four alkaloids isolated from Bulbus of *Fritillaria wabuensis*. *J. Ethnopharmacol.* **2012**, *139*, 189–193. [CrossRef]
17. Hu, J.R.; Jung, C.J.; Ku, S.M.; Jung, D.H.; Ku, S.-K.; Choi, J.S. Antitussive, expectorant, and anti-inflammatory effects of Adenophorae Radix powder in ICR mice. *J. Ethnopharmacol.* **2019**, *239*, 111915. [CrossRef]
18. Hu, J.R.; Jung, C.J.; Ku, S.M.; Jung, D.H.; Bashir, K.M.I.; Ku, S.-K.; Choi, J.-S. Anti-inflammatory, expectorant, and antitussive properties of Kyeongok-go in ICR mice. *Pharm. Biol.* **2021**, *59*, 321–334. [CrossRef]
19. Hu, J.R.; Jung, C.J.; Ku, S.M.; Jung, D.H.; Ku, S.-K.; Mohibbullah, M.; Lee, H.J.; Choi, J.-S. Deciphering the antitussive, expectorant, and anti-inflammatory potentials of Shasham Kyeongok-Go and their phytochemical attributes: In vivo appraisal in ICR mice. *Appl. Sci.* **2021**, *11*, 1349. [CrossRef]
20. Atanasov, A.G.; Zotchev, S.B.; Dirsch, V.M.; Supuran, C.T. Natural products in drug discovery: Advances and opportunities. *Nat. Rev. Drug Discov.* **2021**, *20*, 200–216. [CrossRef]
21. Chaachouay, N.; Zidane, L. Plant-derived natural products: A source for drug discovery and development. *Drugs Drug Candidates* **2024**, *3*, 184–207. [CrossRef]
22. Kim, H.S.; Park, S.I.; Choi, S.H.; Song, C.H.; Park, S.J.; Shin, Y.K.; Han, C.H.; Lee, Y.J.; Ku, S.-K. Single oral dose toxicity test of blue honeysuckle concentrate in mice. *Toxicol. Res.* **2015**, *31*, 61–68. [CrossRef] [PubMed]
23. Negara, B.F.S.P.; Kim, J.W.; Bashir, K.M.I.; Lee, J.-H.; Ku, M.-U.; Kim, K.-Y.; Shin, S.; Hong, E.-J.; Ku, S.-K.; Choi, J.-S. Expectorant effects of immature Asian pear extract on PM2.5-induced subacute pulmonary injury in mice. *J. Food Biochem.* **2023**, *2023*, 5671679. [CrossRef]
24. Ku, S.-K.; Kim, J.W.; Cho, H.R.; Kim, K.Y.; Min, Y.H.; Park, J.H.; Kim, J.S.; Park, J.H.; Seo, B.I.; Roh, S.S. Effect of β-glucan originated from *Aureobasidium pullulans* on asthma induced by ovalbumin in mouse. *Arch. Pharm. Res.* **2012**, *35*, 1073–1081. [CrossRef]
25. Paleari, D.; Rossi, G.A.; Nicolini, G.; Olivieri, D. Ambroxol: A multifaceted molecule with additional therapeutic potentials in respiratory disorders of childhood. *Exp. Opin. Drug Discov.* **2011**, *6*, 1203–1214. [CrossRef]
26. Molina, G.; Holguin, E.; Teran, E. Oral ambroxol supplement in pregnant women induces fetal lung maturation. *Am. J. Obstet. Gynecol.* **2004**, *191*, 2177. [CrossRef]
27. Hong, M.H.; Kim, J.H.; Bae, H.; Lee, N.Y.; Shin, Y.C.; Kim, S.H.; Ko, S.G. *Atractylodes japonica* Koidzumi inhibits the production of proinflammatory cytokines through inhibition of the NF-kappaB/IkappaB signal pathway in HMC-1 human mast cells. *Arch. Pharm. Res.* **2010**, *33*, 843–851. [CrossRef]
28. Wang, K.T.; Chen, L.G.; Chou, D.S.; Liang, W.L.; Wang, C.C. Anti-Oxidative abilities of essential oils from *Atractylodes ovata* rhizome. *eCAM* **2011**, *2011*, 204892. [CrossRef]
29. Han, Y.; Jung, H.W.; Park, Y.K. The roots of *Atractylodes japonica* Koidzumi promote adipogenic differentiation via activation of the insulin signaling pathway in 3T3-L1 cells. *BMC Complement. Altern. Med.* **2012**, *12*, 154. [CrossRef]
30. Rui, M.; Chou, G. Three new polyacetylenes from *Atractylodes japonica* Koidz.ex Kitam. *Nat. Prod. Res.* **2022**, *36*, 2063–2070. [CrossRef]
31. Chen, L.G.; Jan, Y.S.; Tsai, P.W.; Norimoto, H.; Michihara, S.; Murayama, C.; Wang, C.C. Anti-inflammatory and antinociceptive constituents of *Atractylodes japonica* Koidzumi. *J. Agric. Food Chem.* **2016**, *64*, 2254–2262. [CrossRef] [PubMed]
32. Park, S.M.; Lee, S.H.; Jeong, D.U.; Cho, S.-J.; Shin, M.-R.; Roh, S.-S. Antioxidant effect of *Atractylodes macrocephala* Koidzumi in DSS-induced ulcerative colitis model. *Korea J. Herbol.* **2022**, *37*, 19–29.
33. Zhen, B.X.; Cai, Q.; Li, F. Chemical components and protective effects of *Atractylodes japonica* Koidz. ex Kitam against acetic acid-induced gastric ulcer in rats. *World J. Gastroenterol.* **2023**, *29*, 5848–5864. [CrossRef]
34. Deng, X.; Rui, W.; Zhang, F.; Ding, W. PM2.5 induces Nrf2-mediated defense mechanisms against oxidative stress by activating PIK3/AKT signaling pathway in human lung alveolar epithelial A549 cells. *Cell Biol. Toxicol.* **2013**, *29*, 143–157. [CrossRef]

35. Jin, Y.; Wu, W.; Zhang, W.; Zhao, Y.; Wu, Y.; Ge, G.; Ba, Y.; Guo, Q.; Gao, T.; Chi, X.; et al. Involvement of EGF receptor signaling and NLRP12 inflammasome in fine particulate matter-induced lung inflammation in mice. *Environ. Toxicol.* **2017**, *32*, 1121–1134. [CrossRef]
36. Livak, K.J.; Schmittgen, T.D. Analysis of relative gene expression data using real-time quantitative PCR and the 2(−Delta Delta C(T)) method. *Methods* **2001**, *25*, 402–408. [CrossRef]
37. Min, B.G.; Park, S.M.; Choi, Y.W.; Ku, S.-K.; Cho, I.J.; Kim, Y.W.; Byun, S.H.; Park, C.A.; Park, S.J.; Na, M.; et al. Effects of *Pelargonium sidoides* and Coptis Rhizoma 2:1 mixed formula (PS + CR) on ovalbumin-induced asthma in mice. *eCAM* **2020**, *2020*, 9135637. [CrossRef]
38. André, D.M.; Horimoto, C.M.; Calixto, M.C.; Alexandre, E.C.; Antunes, E. Epigallocatechin-3-gallate protects against the exacerbation of allergic eosinophilic inflammation associated with obesity in mice. *Int. Immunopharmacol.* **2018**, *62*, 212–219. [CrossRef]
39. Phung, C.D.; Pham, T.T.; Nguyen, H.T.; Nguyen, T.T.; Ou, W.; Jeong, J.H.; Choi, H.G.; Ku, S.-K.; Yong, C.S.; Kim, J.O. Anti-CTLA-4 antibody-functionalized dendritic cell-derived exosomes targeting tumor-draining lymph nodes for effective induction of antitumor T-cell responses. *Acta Biomater.* **2020**, *115*, 371–382. [CrossRef]
40. Poudel, K.; Park, S.; Hwang, J.; Ku, S.-K.; Yong, C.S.; Kim, J.O.; Byeon, J.H. Photothermally Modulatable and structurally disintegratable sub-8-nm Au1Ag9 Embedded nanoblocks for combination cancer therapy produced by plug-in assembly. *ACS Nano* **2020**, *14*, 11040–11054. [CrossRef]
41. Sauder, D.C.; DeMars, C.E. An updated recommendation for multiple comparisons. *Adv. Methods Pract. Psychol. Sci.* **2019**, *2*, 26–44. [CrossRef]
42. Choi, B.R.; Kim, H.J.; Lee, Y.J.; Ku, S.-K. Anti-diabetic obesity effects of *Wasabia japonica* Matsum leaf extract on 45% Kcal high-fat diet-fed mice. *Nutrients* **2020**, *12*, 2837. [CrossRef] [PubMed]
43. Choi, E.H.; Chun, Y.S.; Kim, J.K.; Ku, S.-K.; Jeon, S.W.; Park, T.S.; Shim, S.M. Modulating lipid and glucose metabolism by glycosylated kaempferol rich roasted leaves of *Lycium chinense* via upregulating adiponectin and AMPK activation in obese mice-induced type 2 diabetes. *J. Funct. Foods* **2020**, *72*, 104072. [CrossRef]
44. Zhou, J.; Han, L.; Ling, Y.; Wang, L.; Li, N.B.; Luo, H.Q. A visual detection of human immunodeficiency virus gene using ratiometric method enabled by phenol red and target-induced catalytic hairpin assembly. *Talanta* **2020**, *219*, 121202. [CrossRef]
45. Tajima, Y. *Biological Reference Data Book on Experimental Animals*; Soft Science Inc.: Tokyo, Japan, 1989.
46. Paliwal, S.; Sudan, V.; Shanker, D.; Srivastava, M. Rapid diagnosis of *Theileria annulata* by colorimetric loop-mediated isothermal amplification (LAMP) assay. *Vet. Parasitol.* **2020**, *285*, 109224. [CrossRef]
47. Liu, X.; Jiang, Y.; Jia, X.; Ma, X.; Han, C.; Guo, N.; Peng, Y.; Liu, H.; Ju, Y.; Luo, X.; et al. Identification of distinct clinical phenotypes of acute respiratory distress syndrome with differential responses to treatment. *Crit. Care* **2021**, *25*, 320. [CrossRef]
48. Tonetti, T.; Pisani, L.; Cavalli, I.; Vega, M.L.; Maietti, E.; Filippini, C.; Nava, S.; Ranieri, V.M. Extracorporeal carbon dioxide removal for treatment of exacerbated chronic obstructive pulmonary disease (ORION): Study protocol for a randomized controlled trial. *Trials* **2021**, *22*, 718. [CrossRef]
49. Na, H.G.; Kim, Y.D.; Choi, Y.S.; Bae, C.H.; Song, S.Y. Diesel exhaust particles elevate MUC5AC and MUC5B expression via the TLR4-mediated activation of ERK1/2, p38 MAPK, and NF-κB signaling pathways in human airway epithelial cells. *Biochem. Biophys. Res. Commun.* **2019**, *512*, 53–59. [CrossRef]
50. Wang, J.; Li, Y.; Zhao, P.; Tian, Y.; Liu, X.; He, H.; Jia, R.; Oliver, B.G.; Li, J. Exposure to air pollution exacerbates inflammation in rats with preexisting COPD. *Mediat. Inflamm.* **2020**, *2020*, 4260204. [CrossRef]
51. Rose, M.C.; Nickola, T.J.; Voynow, J.A. Airway mucus obstruction: Mucin glycoproteins, MUC gene regulation and goblet cell hyperplasia. *Am. J. Respir. Cell Mol. Biol.* **2001**, *25*, 533–537. [CrossRef]
52. Kim, D.H.; Chu, H.S.; Lee, J.Y.; Hwang, S.J.; Lee, S.H.; Lee, H.M. Up-regulation of MUC5AC and MUC5B mucin genes in chronic rhinosinusitis. *Arch. Otolaryngol. Head Neck Surg.* **2004**, *130*, 747–752. [CrossRef] [PubMed]
53. Ballard, S.T.; Spadafora, D. Fluid secretion by submucosal glands of the tracheobronchial airways. *Respir. Physiol. Neurobiol.* **2007**, *159*, 271–277. [CrossRef] [PubMed]
54. Liu, H.; Fan, X.; Wang, N.; Zhang, Y.; Yu, J. Exacerbating effects of PM2.5 in OVA-sensitized and challenged mice and the expression of TRPA1 and TRPV1 proteins in lungs. *J. Asthma* **2017**, *54*, 807–817. [CrossRef]
55. Ji, Z.; Wang, Z.; Chen, Z.; Jin, H.; Chen, C.; Chai, S.; Lv, H.; Yang, L.; Hu, Y.; Dong, R.; et al. Melatonin attenuates chronic cough mediated by oxidative stress via transient receptor potential melastatin-2 in guinea pigs exposed to particulate matter 2.5. *Physiol. Res.* **2018**, *67*, 293–305. [CrossRef]
56. Weldy, C.S.; Luttrell, I.P.; White, C.C.; Morgan-Stevenson, V.; Cox, D.P.; Carosino, C.M.; Larson, T.V.; Stewart, J.A.; Kaufman, J.D.; Kim, F.; et al. Glutathione (GSH) and the GSH synthesis gene Gclm modulate plasma redox and vascular responses to acute diesel exhaust inhalation in mice. *Inhal. Toxicol.* **2013**, *25*, 444–454. [CrossRef]

57. Fan, R.; Ren, Q.; Zhou, T.; Shang, L.; Ma, M.; Wang, B.; Xiao, C. Determination of endogenous substance change in PM2.5-induced rat plasma and lung samples by UPLC-MS/MS method to identify potential markers for lung impairment. *Environ. Sci. Pollut. Res. Int.* **2019**, *26*, 22040–22050. [CrossRef]
58. Tumes, D.J.; Cormie, J.; Calvert, M.G.; Stewart, K.; Nassenstein, C.; Braun, A.; Foster, P.S.; Dent, L.A. Strain-dependent resistance to allergen-induced lung pathophysiology in mice correlates with rate of apoptosis of lung-derived eosinophils. *J. Leukoc. Biol.* **2007**, *81*, 1362–1373. [CrossRef]
59. Tillie-Leblond, I.; Gosset, P.; Le Berre, R.; Janin, A.; Prangère, T.; Tonnel, A.B.; Guery, B.P. Keratinocyte growth factor improves alterations of lung permeability and bronchial epithelium in allergic rats. *Eur. Respir. J.* **2007**, *30*, 31–39. [CrossRef]
60. Choi, H.Y.; Jung, T.Y.; Ku, S.-K.; Yang, H.B.; Lee, H.S. Toxico-pathological study of p,p-DDE after experimental aerosol exposed to ICR Mouse. *Toxicol. Res.* **2005**, *21*, 151–160.
61. Honda, H.; Fujimoto, M.; Miyamoto, S.; Ishikawa, N.; Serada, S.; Hattori, N.; Nomura, S.; Kohno, N.; Yokoyama, A.; Naka, T. Sputum Leucine-rich alpha-2 glycoprotein as a marker of airway inflammation in asthma. *PLoS ONE* **2016**, *11*, e0162672. [CrossRef]
62. Chen, Y.C.; Shen, S.C.; Lee, W.R.; Hsu, F.L.; Lin, H.Y.; Ko, C.H.; Tseng, S.W. Emodin induces apoptosis in human promyeloleukemic HL-60 cells accompanied by activation of caspase 3 cascade but independent of reactive oxygen species production. *Biochem. Pharmacol.* **2002**, *64*, 1713–1724. [CrossRef] [PubMed]
63. Wang, A.S.; Xu, Y.; Zhang, Z.W.; Lu, B.B.; Yin, X.; Yao, A.J.; Han, L.Y.; Zou, Z.Q.; Li, Z.; Zhang, X.H. Sulforaphane protects MLE-12 lung epithelial cells against oxidative damage caused by ambient air particulate matter. *Food Funct.* **2017**, *8*, 4555–4562. [CrossRef] [PubMed]
64. Wang, Y.; Zhao, B.; Fei, Y.; Yin, Q.; Zhu, J.; Ren, G.; Wang, B.; Fang, W.; Li, Y. Ma xing shi gan decoction eliminates PM2.5-induced lung injury by reducing pulmonary cell apoptosis through Akt/mTOR/p70S6K pathway in rats. *Biosci. Rep.* **2020**, *40*, BSR20193738. [CrossRef] [PubMed]
65. Li, X.; Ding, Z.; Zhang, C.; Zhang, X.; Meng, Q.; Wu, S.; Wang, S.; Yin, L.; Pu, Y.; Chen, R. MicroRNA-1228(*) inhibit apoptosis in A549 cells exposed to fine particulate matter. *Environ. Sci. Pollut. Res. Int.* **2016**, *23*, 10103–10113. [CrossRef]
66. He, M.; Ichinose, T.; Yoshida, S.; Ito, T.; He, C.; Yoshida, Y.; Arashidani, K.; Takano, H.; Sun, G.; Shibamoto, T. PM2.5-induced lung inflammation in mice: Differences of inflammatory response in macrophages and type II alveolar cells. *J. Appl. Toxicol.* **2017**, *37*, 1203–1218. [CrossRef]
67. Zou, C.; Yang, H.; Cui, L.; Cao, X.; Huang, H.; Chen, T. Potential hazardous effects of printing room PM2.5 exposure include promotion of lung inflammation and subsequent injury. *Mol. Med. Rep.* **2020**, *22*, 3213–3224. [CrossRef]
68. Mohy El-Din, M.M.; Senbel, A.M.; Bistawroos, A.A.; El-Mallah, A.; Nour El-Din, N.A.; Bekhit, A.A.; Abd El Razik, H.A. A novel COX-2 inhibitor pyrazole derivative proven effective as an anti-inflammatory and analgesic drug. *Basic Clin. Pharmacol. Toxicol.* **2011**, *108*, 263–273. [CrossRef]
69. Hamsa, T.P.; Kuttan, G. Evaluation of the anti-inflammatory and anti-tumor effect of *Ipomoea obscura* (L) and its mode of action through the inhibition of proinflammatory cytokines, nitric oxide and COX-2. *Inflammation* **2011**, *34*, 171–183. [CrossRef]
70. Wang, F.; Wang, R.; Liu, H. The acute pulmonary toxicity in mice induced by *Staphylococcus aureus*, particulate matter, and their combination. *Exp. Anim.* **2019**, *68*, 159–168. [CrossRef]
71. Wang, P.; Liu, H.; Fan, X.; Zhu, Z.; Zhu, Y. Effect of San'ao decoction on aggravated asthma mice model induced by PM2.5 and TRPA1/TRPV1 expressions. *J. Ethnopharmacol.* **2019**, *236*, 82–90. [CrossRef]
72. Zhao, C.; He, C. Preparative isolation and purification of atractylon and atractylenolide III from the Chinese medicinal plant *Atractylodes macrocephala* by high-speed counter-current chromatography. *J. Sep. Sci.* **2006**, *29*, 1630–1636. [CrossRef] [PubMed]
73. Lee, H.; Im, H.J.; Lim, H.; Kim, H.P.; Kim, J.; Kim, J.S. Anti-allergic effects of the rhizomes of *Atractylodes japonica* and the main constituents. In Proceedings of the 2012 International Conference on Biomedical Engineering and Biotechnology, Macao, 28–30 May 2012; pp. 57–59.
74. Kim, J.-H. Pharmacokinetic analysis of atractylenolide III in rat plasma after oral administration of *Atractylodes japonica* rhizome extract by ultra-performance liquid chromatography-ion trap mass spectrometry. *Acta Chromatogr.* **2019**, *31*, 266–271. [CrossRef]
75. Kim, J.H.; Lee, Y.; Lee, G.; Doh, E.-J.; Hong, S. Quantitative interrelation between atractylenolide I, II, and III in *Atractylodes japonica* Koidzumi rhizomes, and evaluation of their oxidative transformation using a biomimetic kinetic model. *ACS Omega* **2018**, *3*, 14833–14840. [CrossRef] [PubMed]
76. Chae, H.-S.; Kim, S.Y.; Pel, P.; Huh, J.; Joo, S.-W.; Lim, Y.Y.; Park, S.J.; Lim, J.L.; Chin, Y.-W. Standardized extract of Atractylodis Rhizoma Alba and Fructus Schisandrae ameliorates coughing and increases expectoration of phlegm. *Molecules* **2020**, *25*, 3064. [CrossRef] [PubMed]

Disclaimer/Publisher's Note: The statements, opinions and data contained in all publications are solely those of the individual author(s) and contributor(s) and not of MDPI and/or the editor(s). MDPI and/or the editor(s) disclaim responsibility for any injury to people or property resulting from any ideas, methods, instructions or products referred to in the content.